Chem Soc Rev

Cite this: *Chem. Soc. Rev.*, 2012, **41**, 6631–6662

www.rsc.org/csr

CRITICAL REVIEW

Exploring the complexity of aerosol particle properties and processes using single particle techniques†

Ulrich K. Krieger,[a] Claudia Marcolli[a] and Jonathan P. Reid*[b]

Received 16th March 2012
DOI: 10.1039/c2cs35082c

The complex interplay of processes that govern the size, composition, phase and morphology of aerosol particles in the atmosphere is challenging to understand and model. Measurements on single aerosol particles (2 to 100 μm in diameter) held in electrodynamic, optical and acoustic traps or deposited on a surface can allow the individual processes to be studied in isolation under controlled laboratory conditions. In particular, measurements can now be made of particle size with unprecedented accuracy (sub-nanometre) and over a wide range of timescales (spanning from milliseconds to many days). The physical state of a particle can be unambiguously identified and its composition and phase can be resolved with a high degree of spatial resolution. In this review, we describe the advances made in our understanding of aerosol properties and processes from measurements made of phase behaviour, hygroscopic growth, morphology, vapour pressure and the kinetics of water transport for single particles. We also show that studies of the oxidative aging of single particles, although limited in number, can allow the interplay of these properties to be investigated. We conclude by considering the contributions that single particle measurements can continue to make to our understanding of the properties and processes occurring in atmospheric aerosol.

I. Introduction

The analysis of ambient aerosol often starts with a measurement of the particle size distribution. Although this can be indicative of source and lifetime, the importance of characterising composition is now well-established for inferring key properties of the aerosol such as hygroscopicity and the activity of cloud condensation

[a] *Institute for Atmospheric and Climate Science, ETH Zurich, Zurich, Switzerland*
[b] *School of Chemistry, University of Bristol, Cantock's Close BS8 1TS Bristol, U.K. E-mail: j.p.reid@bristol.ac.uk*
† Part of the atmospheric chemistry themed issue.

Ulrich K. Krieger

Ulrich K. Krieger is currently a senior scientist at the Institute for Atmospheric and Climate Science at ETH Zurich (Switzerland). With laboratory experiments he performs research on aerosol microphysics and chemistry. He studied physics at the University of Würzburg (Germany) and the State University of New York at Albany (USA). In 1994 he received his PhD for experimental work on non-classical light scattering in water from the Technical University of Berlin (Germany). In 1995 he joined the Max-Planck-Institute for Chemistry in Mainz (Germany), where he started using single particle techniques for studying atmospheric aerosol.

Claudia Marcolli

Claudia Marcolli works as a senior scientist at the Institute for Atmospheric and Climate Science at ETH Zurich (Switzerland). Her current research interests are the microphysical properties of atmospheric aerosols and clouds with focus on ice nucleation, liquid–liquid phase separation and glass formation. She studied chemistry at the University of Bern (Switzerland) and received her PhD in 1996. Thereafter, she was first employed at Novartis Services AG and then at Solvias AG investigating solid state properties of active substances. In 2002 she joined the research group of Prof. Thomas Peter at ETH Zurich.

nuclei (CCN) and ice nuclei (IN).[1,2] With the organic components often exceeding 50% of the condensed phase mass,[3–5] representing the properties of the aerosol by considering the inorganic components alone is misleading. For example, although inorganic compounds invariably show hysteresis in their deliquescence/efflorescence behaviour, organic compounds can either show discrete phase behaviour or are often observed to absorb and desorb water continuously with change in relative humidity (RH).[6–10] The organic fraction, which consists of a myriad of different compounds,[11] is frequently sub-divided according to component properties, such as water solubility, volatility and efficiency at absorbing light.[12–14] Given the considerable variation in water solubility of the organic components and considering the interactions with internally mixed inorganic components, individual aerosol particles can be composed of more than a single phase, with a solid inclusion in a liquid host droplet, liquid–liquid phase separation or even multiple solid phase domains.[15–17] Even individual phase domains may be heterogeneous rather than homogeneous in composition.[18–20] Clearly, the properties of atmospheric aerosol can be resolved at varying levels of complexity, starting with a simple measurement of size and extending through to the characterisation of the composition and morphology of individual phase domains.

Justifiably, an important question must be asked: at what level of detail is it necessary to resolve the complexity in the microphysical state, the chemical makeup, and the processing of an aerosol particle to understand both the forcings and feedbacks of aerosols on climate and their impact on atmospheric composition? A less ambitious question, but one that serves as an important first step to addressing the more general one, is to ask what influence the physical state and the chemical makeup have on both the properties of the aerosol and the processes that transform it? If for a given chemical composition, the physical properties and timescales of transformation are quantified through controlled laboratory measurements, answering this second question may provide invaluable insight into how the former question should be answered. However, answering the former question does rely on atmospheric modelling studies, for which simple parameterisations of laboratory data are crucial. In this review we will focus on the second of these two questions, highlighting the ways in which controlled laboratory studies can provide insight into aerosol properties and processes of potential atmospheric importance and their dependence on the physical state and chemical composition of the aerosol.

Examining the links between the timescales for transformation processes and the microphysical state and chemical composition of ambient particles is challenging as both the aerosol and gas phase concentrations of key species can be highly variable in space and time and it is impossible to fully characterise all of the key parameters that must be known. By contrast, laboratory measurements (*e.g.* smog chamber, flow reactor, single particle measurements) allow the control of key variables such as RH, temperature, oxidant concentration, particle size, composition and concentration, and light irradiance. In addition, interrogating the 'same' aerosol at various points in time is facile, allowing time-dependent processes to be explored.

There are a number of notable advantages of studying aerosol processes on a single particle basis. Firstly, it is possible to observe directly the microphysical state of the aerosol, identifying different liquid and crystalline phase domains.[6,21–24] The size and chemical composition of the aerosol can often be directly interrogated by non-intrusive techniques such as elastic light scattering and Raman spectroscopy.[25–28] Measurements can be made on the same particle over a period of time while environmental conditions are readily varied and the response of the aerosol recorded *in situ*. There are numerous experimental approaches to studying aerosols on a single particle basis including optical levitation and optical tweezers,[27,29–32] the electrodynamic balance,[33–35] the acoustic trap[36–38] and microscopy of particles deposited on surfaces.[39–42] The purpose of this review is not to discuss these approaches in detail, although their applications will be identified. Further, we do not attempt to provide a comprehensive account of the full range of experimental studies that have been performed, but rather to highlight a small subset that illustrate how single particle techniques can be applied to study aerosol processes and properties.

The connections between the microphysical state and chemical makeup of a particle with the transformation processes are summarised in Fig. 1. The complex phase behaviour and microphysical structure/morphology of an aerosol consisting of inorganic salts and a mixture of organic hydrophilic and hydrophobic components is indicated in the central yellow shaded region. A particle can consist of separated liquid[17,24,43] or crystalline phases[22] or can exist in a liquid or amorphous/glassy one-phase state.[44–47] Phases are homogeneous in composition when their viscosity is low and diffusion over the lengthscale of particle diameter is fast compared with the timescale of processing, but may be heterogeneous on a much finer lengthscale for highly viscous or glassy particles.

The chemical composition and microphysical state influence the response of the particle to environmental changes as indicated by the arrows in Fig. 1. By changing RH and temperature, both the thermodynamic and kinetic response of the particle can be probed. For example, a reduction in RH leads to a reduction in the equilibrium mass of condensed

Jonathan P. Reid

Jonathan Reid is a Professor of Physical Chemistry at the University of Bristol (UK). His work focuses on the application of single particle trapping and spectroscopic techniques for studying aerosol properties and processes of relevance to the atmosphere, drug delivery to the lungs and spray drying. He studied for his MA (1994) and DPhil (1997) in Chemistry at the University of Oxford before a period as a post-doctoral researcher at JILA, University of Colorado (USA). He returned to the UK as a lecturer in 2000 at the University of Birmingham, moving to Bristol in 2004. He is currently an EPSRC Leadership Fellow.

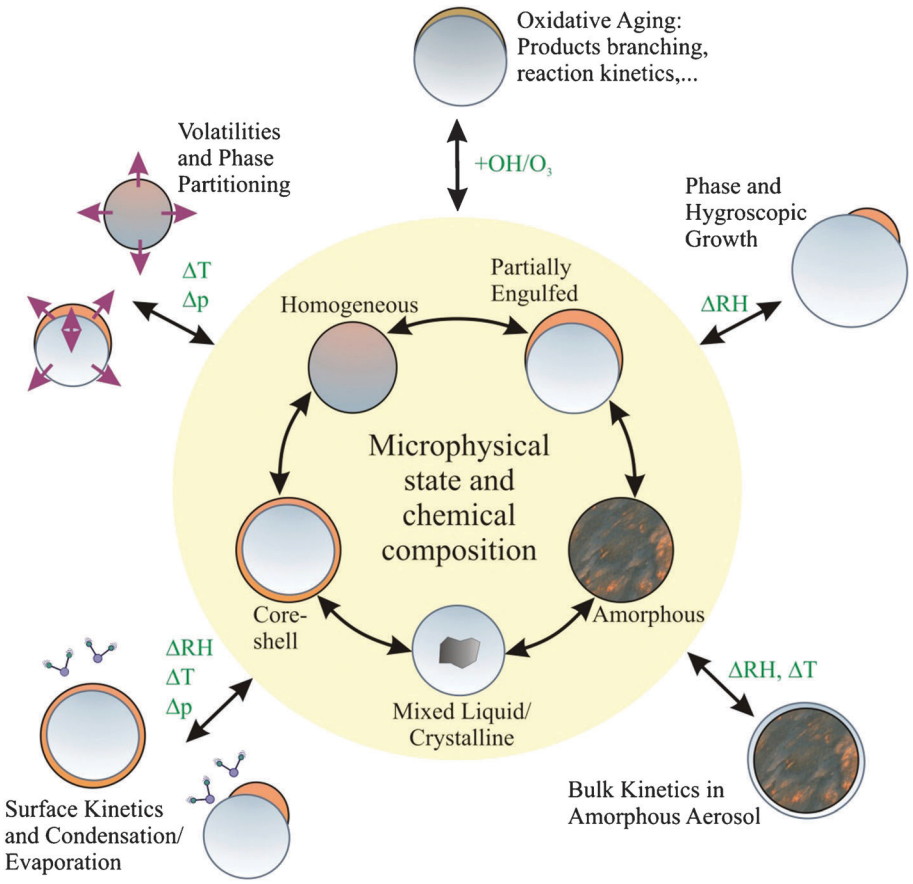

Fig. 1 Schematic illustrating key aerosol processes and their relationship to the microphysical state of the aerosol particle. It should be noted that even crystalline solid phases can exist in a range of polymorphic forms.

phase water and the size of the aqueous phase volume, and may induce phase changes like liquid–liquid phase separation and efflorescence.[6,7] In contrast, the non-equilibrium kinetically limited response to change in environmental conditions can be dependent on metastable amorphous phases exhibiting delayed response to changes in RH.[45,46,48,49] Further, surface kinetics such as the accommodation of water may be dependent on the microphysical state and chemical composition; indeed, the kinetics of activation of aerosol as CCN or IN may be governed by the existence of a monomolecular film of surface active organic components on the surface of a growing cloud droplet or ice crystal.[50–52]

At constant RH and temperature, particle contraction is indicative of evaporation of semi-volatile compounds (SVOCs) and can be used to determine the vapour pressure of a chemical component.[53,54] Vapour pressures depend on the physical state of a system and so a correct evaluation is dependent on a correct assignment of the particle phase to a specific physical state.[55] Consequently, the phase state of the particle must be monitored during the experiment and diffusion limitations during the experiment must be excluded. Exposing the particle to oxidative vapours, heterogeneous chemistry and chemical processing can be investigated.[56,57] The reaction kinetics and product branching of oxidative processing may be different for organic components externally and internally mixed with inorganic seeds.[2,58–60] Certainly, the presence of a deliquesced seed can open up the possibility that condensed aqueous phase chemistry can occur as well as organic phase reactions, and can modify the surface-to-volume ratio of the organic phase volume, influencing reaction kinetics.[61]

Although a reductionist view, which defines the key relationships between properties and processes in the way shown in Fig. 1, can be helpful in resolving uncertainties in a systematic way, it must be remembered a complex interplay exists between all of the properties and processes in any real situation. A key bridge between individual process studies and the complexity found in the atmosphere can be provided by single particle studies. For example, the equilibrium hygroscopic response and kinetic limitations to water transport, component vapour pressures and reaction product branching can be retrieved prior to and post oxidative aging for the same particle.[56,57,61]

In this review, we consider how single particle measurements can allow us to explore the individual processes identified in Fig. 1. After introducing some of the experimental techniques that are commonly used, we discuss the hygroscopicity, morphology and phase behaviour together as these are clearly linked and form the basis for understanding the other processes defined in Fig. 1. We then examine the gas-particle partitioning of SVOCs, the kinetics of surface and bulk processes, and the oxidative aging kinetics and mechanism for organic components. Finally, we conclude by considering how such measurements made at the single particle level could allow us to interrogate the full complexity of aerosol properties and processes that occur in the atmosphere.

II. Experimental techniques

We will briefly review the experimental techniques that can be used for isolating individual particles and the methods available for analysing particle size, composition and morphology. Examples of the four experimental techniques that will be described are shown in Fig. 2.

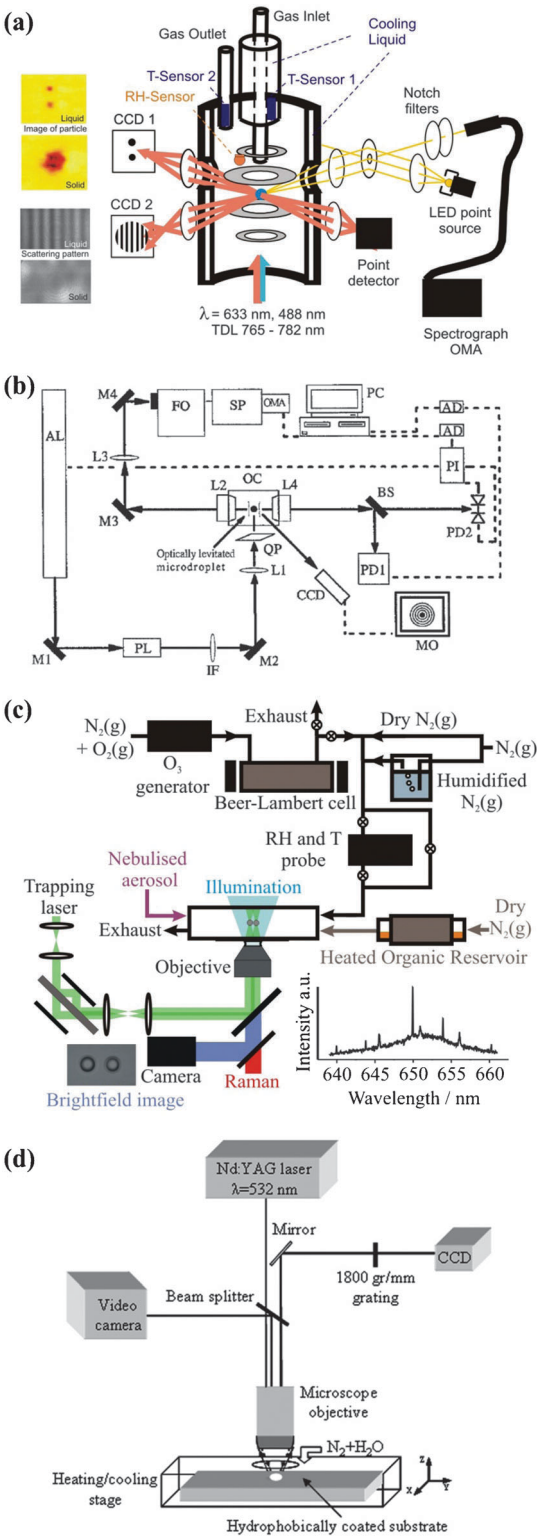

II.a Isolating single particles

There are already numerous reviews[27,33,62,63] that focus on the techniques used for isolating and capturing single particles and we will not provide a comprehensive account here. Instead, we will briefly highlight the key techniques that underpin the aerosol measurements that are described in later sections. The techniques can be broadly classified as electrodynamic, optical or surface based in the method used to isolate individual particles. Acoustic traps will not be described here as they are limited to particles that are larger than 20 μm in diameter, an upper limit on particle size for the studies of properties by other techniques reviewed here.[37,64]

The use of charge and electric fields to isolate particles has a history that goes back to the classical Millikan oil drop experiments in the early 20th century.[65,66] However, considerable advances have been made in the delivery of particles and in the stability that can be achieved in particle position, using not just a DC field to counter the gravitational force acting on a charged particle but providing a restoring force with an AC field that allows tight confinement of position of a particle in the horizontal plane.[67,68] Numerous designs for electrodynamic balances (EDBs) have been developed, ranging from a simple two electrode ring design to the more complex standard hyperboloidal electrodynamic levitator.[33,34] Each design varies in the strength of the restoring force acting on a particle to the degree of optical access for light scattering measurements. Often housed within a vacuum chamber, the gas composition can be varied allowing control over RH and temperature, and the introduction of gas phase reactants. The size of the chamber and the moderate gas flow can limit the response time to changes in gas phase composition, with a typical exponential response in RH of minutes at room temperature and up to several hours at 200 K.[49] Recently, a concentric cylindrical electrode EDB has been used to trap particles in a rapidly flowing gas stream, allowing reproducible measurements in conditions that can be radically altered on a few second timescale.[69,70] Typical EDB measurements are performed on particles from 5 to 50 μm radius and either solid or liquid. Droplets can be readily loaded from piezoelectric or thermal bubble driven droplet-on-demand generators. Changes in mass

Fig. 2 Schematic diagrams of (a) an electrodynamic balance setup; a hyperboloidal quadrupole trap is housed in a three wall glass chamber, CCD1 records the microscopic image of the particle, CCD2 its phase function, Mie resonance spectra or Raman spectra are recorded with a fibre coupled spectrograph, OMA optical multichannel analyser, TDL tuneable diode laser [Reprinted with permission from ref. 49, Copyright Royal Society of Chemistry]; (b) an optical levitation experiment, AL argon-ion laser, M1–M4 mirrors, PL polarizer, IF interference filter, L1–L4 lenses, QP single-crystal quartz plate, OC observation chamber, PD photodiodes, BS beamsplitter, PI proportional integral feedback system, AD analog-to-digital converter, FO fore-monochromator, SP spectrograph, OMA optical multichannel array, PC computer, CCD camera, MO monitor [Reprinted with permission from ref. 77, Copyright Applied Spectroscopy, Allen Press]; (c) aerosol optical tweezers [Adapted with permission from ref. 61, Copyright 2012 American Chemical Society.]; and (d) a microRaman instrument [Adapted with permission from ref. 43, Copyright 2009 American Chemical Society.]

of the particle can be measured over time, often measured relative to the mass of the particle under dry (RH < 5%) conditions. In addition, particles can be characterised by elastic light scattering and by Raman spectroscopy[71] or laser induced fluorescence.[72] These spectroscopic tools can be similarly applied to the techniques described below.

Optical methods for isolating single droplets can be divided into two types, countering the action of gravity with backwards light scattering using a vertically propagating laser beam[73–79] or exerting a strong gradient restoring force on a particle to the region of highest light intensity in a single-beam gradient force optical trap, also referred to as optical tweezers.[31,32,80] The former can be considered equivalent to exerting a push on a particle along the beam propagation direction, while the latter is equivalent to exerting a pull on a particle. Ashkin and Dziedzic first demonstrated that glass beads, ~20 μm in diameter, could be levitated in a gently focussed laser beam,[30] following this soon after by reporting the levitation of liquid droplets.[81] The height at which the particle sits in the vertically propagating beam is determined by a balance of the optical and gravitational forces. Changes in droplet size by evaporation, condensation or phase transition must be accompanied by active changes in the light intensity to retain a trapped particle. Measurements can be routinely made on droplets 20–100 μm in diameter held within a temperature and RH controlled environment.[79,82,83] Optical tweezers provide a more robust trap with the gradient force typically many orders of magnitude larger than the scattering and gravitational forces, leading to true 3-dimensional confinement in position with a single laser beam.[84,85] Droplets 1–10 μm radius can be routinely studied with this approach and can be held within a gas flow and to low pressure (~2 kPa).[32,86,87] The optical trap can be loaded from a standard ultrasonic nebuliser or using droplet-on-demand generators.[88] The gradient trap is limited to particles that are approximately spherical in shape, although crystalline, solid, and aspherical particles can be still studied.[48,86,89–91] Arrays of aerosol droplets can be manipulated in real time using holographic optical tweezers.[92,93] Combining the scattering and gradient forces characteristic of optical levitation and tweezers, Bessel beam can be configured in either vertically or horizontally trapping arrangements and provide an approach for trapping sub-μm particles.[94–96]

A third strategy for studying immobilised particles is to deposit them on a surface.[20,21,41–43,97] Such an approach is often coupled with conventional brightfield microscopy and Raman spectroscopy, giving the top view of the particle and allowing its composition to be interrogated with spatial resolution. A typical setup is sketched in Fig. 2(d). With confocal Raman microscopy, one can gain in addition information on the particle composition in the third dimensions (*i.e.* z-coordinate). Aqueous solution droplets are usually deposited on a hydrophobic surface preventing the uniform spreading of the droplet over the substrate. Indeed, super-hydrophobic surfaces can allow the droplet to retain a shape that does not depart too significantly from sphericity. The droplet on the substrate is placed in a temperature controlled cell with a regulated N_2/H_2O flow going through it to perform humidity cycles. The design of the cell limits the spatial and confocal resolution to several microns because long-working distance objectives are needed to focus on the particle in the cell. This sets the lower limit on the droplet size to a few microns, because phase changes and morphologies of smaller particles cannot be observed unambiguously. One potential flaw of this technique is the influence of the substrate on the measurements. Whether the substrate is indeed an issue depends, however, on the specific type of experiment and the quantities that one derives from it. Normally, thermodynamic properties are less sensitive to the presence of the substrate than kinetic ones such as nucleation. The most delicate topic is the influence of the substrate on the morphology of the particles which we will address in section III.d.

II.b Characterising single particles

Once isolated, non-intrusive techniques must be used to characterise the particle diameter, mass, composition and morphology. The relative changes in mass of a particle can be recorded in an EDB by recording the DC voltage required to compensate for the gravitational force to hold the trapped particle at the null point of the balance, a measure for the mass to charge ratio.[33,62] If small changes in mass must be measured, the technique can suffer from drifts associated with charge loss, drifts in the electric fields or in the feedback electronics to keep the particle at the null point. However, this approach allows the solute concentration to be estimated (in molality units or as the mass fraction of solute) in hygroscopicity experiments without the need for information on any further physical property (such as density) except a bulk concentration reference point (cp. section III.b). Most other techniques for particle characterization are optical, either relying on elastic or inelastic light scattering and these will be the focus of the remainder of this section.

A Raman spectrum can provide an unambiguous signature of the chemical composition of a droplet if Stokes bands from different species are identified.[76–79] Indeed, Raman lineshapes and frequencies can be used to investigate the change in intermolecular interactions with change in composition, for example induced by changes in RH, extending the information that can be gathered beyond the more straightforward determination of solute concentrations.[98,99] Similarly, fluorescence spectroscopy has been used to interrogate the changes in hydrogen bonding within supersaturated solution droplets up to the point of efflorescence.[72]

A common approach to estimating particle radius is from the intensity of elastically scattered laser light recorded as a function of scattering angle, often referred to as the phase function.[100–103] If the particle is assumed to be spherical, this angularly resolved interference pattern can be compared with calculations from Mie theory to retrieve the radius, provided the refractive index is known. Measurements of the elastic light scattering in the rainbow region have been used to estimate both the radius and refractive index of spherical particles.[104]

An approach related to the phase function is to record the resonance spectrum, the intensity of elastically scattered light intensity recorded at a fixed angle over time.[105–109] A micron-sized spherical droplet acts as a very high-quality optical cavity with the cavity modes being referred to as morphology dependent resonances or whispering gallery modes (WGMs).[110,111] When the droplet size is resonant with a WGM at the wavelength of the laser, the intensity of the scattered light increases markedly with scattering at WGM wavelengths being isotropic.

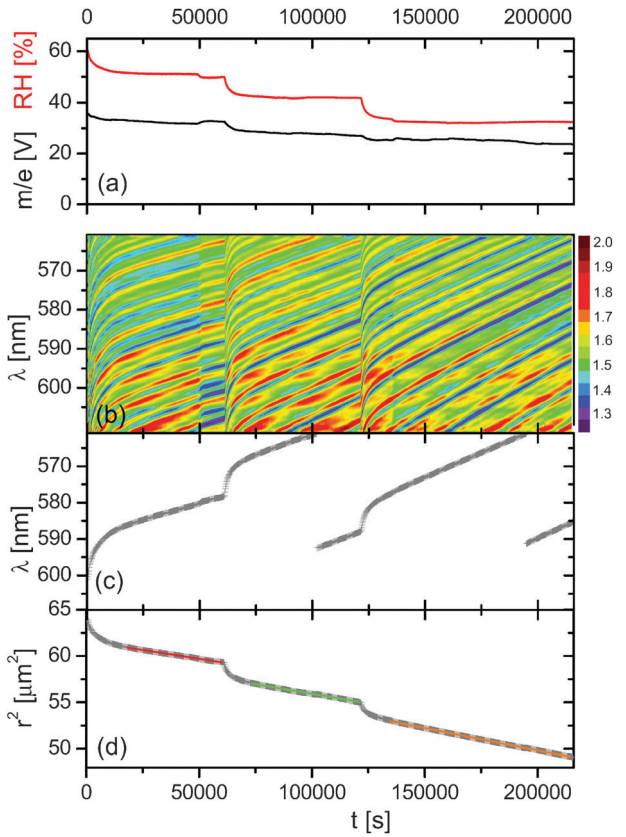

Fig. 3 (a) Experimental data from a vapour pressure measurement of an aqueous malonic acid particle at 291 K exposed to different relative humidities. The DC voltage necessary to balance the gravitational force is shown along with the time dependence of the relative humidity. (b) Colour coded elastic Mie resonance spectra. (c) The tracking of specific resonance wavelengths with time is shown, with the shift to shorter wavelength corresponding to diminishing particle size. Evolving size of the droplet is calculated from this shift and shown in panel (d). The decrease in size arises from both step changes in RH and evaporation of malonic acid during periods of constant RH, with the slopes at constant RH being linear with radius squared and increasing in steepness with lower RH. [Reprinted with permission from ref. 115, Copyright Optical Society of America.]

The resonance spectrum can be compared to computed Mie spectra to obtain size and refractive index.[112] Indeed, this approach has also been used to infer refractive index gradients arising from concentration gradients within evaporating droplets[113] and the thickness of a shell on a core of differing refractive index.[105,114] A variant of Mie resonance spectroscopy was introduced by Zardini *et al.*[115] Instead of using a fixed wavelength source and monitoring the intensity of scattered light with time, they used a broadband LED source in a backscattering configuration to measure scattered intensity resolved as a function of wavelength providing Mie resonance spectra. From the shifts in WGM wavelengths, the variation in particle size with time was estimated, an example of which is shown in Fig. 3.

For spherical droplets, the Raman spectra can also be used to characterise size.[74,75,116,117] At wavelengths commensurate with WGMs within the Stokes shifted bands, a droplet behaves as a low loss optical cavity providing a mechanism for optical feedback and amplification of the inelastically scattered light.[111,118] Thus, broad Raman bands, such as that arising from excitation of the O–H stretching vibration of water, are composed of both a broad underlying band arising from spontaneous Raman scattering and resonant structure arising from stimulated Raman scattering.[116,117,119–121] This is often referred to as cavity enhanced Raman spectroscopy (CERS). In addition to allowing the estimation of droplet size with sub-nanometre accuracy from droplets of known refractive index, the CERS fingerprint provides a unique signature of both the real part of the refractive index and the droplet size and both can be retrieved.[122] The thickness of shells of differing refractive index from a core can also be estimated in the same way as described for an elastic resonance spectrum.[123] As soon as the particle loses spherical symmetry either by partial or complete crystallization or a liquid–liquid phase separation, this change in morphology will show up in the resonance structure in either CERS spectra[24] or elastic Mie resonance spectra and when measuring intensity fluctuations with a point detector.[124]

Most of the light scattering sizing techniques described so far are only strictly applicable to spherical droplets. However, sizing techniques for solid, non-spherical, evaporating particles are needed.[125] Krieger and Zardini[126] used dynamic light scattering to measure the rotational Brownian motion of a solid ammonium nitrate particle evaporating in a nitrogen atmosphere. Zardini and Krieger[127,128] recognized that wavelength dependent elastic scattering spectra of evaporating non-spherical particles after normalization exhibit patterns similar to those of spherical droplets, but somewhat distorted. These patterns allow size changes to be deduced, although with inferior precision to measurements on spherical droplets.

III. Hygroscopicity, morphology and phase behaviour

The hygroscopicity of atmospheric aerosol contributes to the magnitude of the aerosol direct radiative effect on climate. Water uptake increases the particle size and, thus, enhances the ability of the particle to scatter light. Field data show the RH dependence of particle volume[129] is as expected from laboratory experiments. Concurrently with size, hygroscopic growth leads to a change in the refractive index of the particle, influencing the scattering and absorption properties.[129] Most inorganic salts exist as dry particles at low relative humidity (RH) and take up water abruptly at the deliquescence relative humidity, but remain in a metastable liquid state upon drying until the efflorescence humidity is reached with the salt crystallizing. This hysteresis behaviour, in particular, will strongly influence the direct aerosol effect. Laboratory data from single particle studies have therefore been used to predict phase states of aerosol particles in global models (*e.g.* Colberg *et al.*[130] and Martin *et al.*[131]). Wang *et al.*[132] have concluded that the effect of hysteresis for inorganic sulphate aerosol results in an uncertainty of 20% in sulphate direct climate forcing. Organic compounds strongly influence the hygroscopicity and direct effect causing less cooling by the aerosol.[133] Collins *et al.*[134] found agreement within 2.5% between aerosol optical depth determined by an airborne sunphotometer and that calculated from microphysical measurements for clean boundary layer conditions. The discrepancy was larger when dust and

anthropogenic aerosols were present, and was 13% for polluted boundary layer conditions. Not only do the hygroscopic properties of the aerosol influence the direct radiative effect, but also indirectly through influencing the radiative properties of clouds through cloud droplet number, size and lifetime.[1,135] Further, aerosol hygroscopicity also influences the way aerosol particles are chemically altered by gas phase molecules and *vice versa*.[136]

As outlined in the introduction, single particle techniques are useful for both the elucidation of microphysical processes and measurements of basic thermodynamic or kinetic quantities. In particular, they allow access to basic thermodynamic quantities that are not accessible by bulk measurements. We will discuss deliquescence and efflorescence relative humidities first, focusing on organics and their mixtures with atmospherically relevant inorganic salts, summarizing the large body of single particle experimental work in a comprehensive table. We will also exemplify how hygroscopic growth measurements help to parameterize thermodynamic models, discuss liquid–liquid phase separation and polymorphism, and show the unique capability of single particle experiments to investigate the complex morphology of multicomponent aerosol particles.

III.a Efflorescence and deliquescence

When crystalline salt particles are exposed to increasing RH, they take up water at a well-defined specific RH to become solution droplets. This process is called deliquescence and the RH at which it occurs is the deliquescence RH (DRH). At the DRH the particle consists of a saturated salt solution with a water activity (a_w) corresponding to the RH surrounding the particle, ignoring the influence of the Kelvin term on the water vapour pressure. When the same particle is dried, it continuously loses water, becoming a supersaturated solution droplet at RHs below the DRH, and finally crystallizes by releasing water to the gas phase at the efflorescence RH (ERH). Deliquescence and efflorescence can both be investigated on single particles exposed to humidity cycles. With levitated particles in an EDB, mass and radius is monitored (section II.b); in microscopy techniques, the dissolution and crystallization is observed optically, mostly in transmission mode.

While the DRH is a thermodynamic quantity that can be determined by measuring the water activity of saturated salt solutions, efflorescence is initiated by a nucleation process that occurs at a specific rate and therefore depends on timescales and particle size. Often it is assumed that nucleation occurs by a homogeneous nucleation process in the volume of the solution. Particles investigated by single particle techniques are typically larger than ambient aerosol particles and it can be assumed that ambient aerosols can reach the high supersaturation determined by the laboratory measurements of the ERH, possibly even persisting to higher supersaturations.[137] Therefore, these measurements are highly relevant for quantifying the direct aerosol effect.

There exists a large body of literature on deliquescence and efflorescence of salt particles. A comprehensive review on this topic is given by Martin.[138] In this review, we will briefly summarize the results for the common salts that are most important for the atmosphere, namely sodium chloride, ammonium nitrate and ammonium containing sulphate salts. Moreover, the focus will be on the efflorescence process. We will then focus on organic compounds used as model systems for atmospheric aerosols and their mixtures with inorganic salts.

Ammonium sulphate. Table 1 gives a selection of DRH and ERH values that have been measured on single particles of ammonium sulphate and the reader is referred to the Table for a detailed list of publications. Deliquescence of ammonium sulphate occurs at ~80% RH. For efflorescence, a range from 34–48% RH is reported in literature from EDB and microscopy experiments. Somewhat lower values down to ~30% RH have been observed by single particle measurements in flow tube systems.[142] Some single particle studies have attempted more detailed and quantitative evaluation of ERH that illustrate the potential of single particle techniques for elucidating the mechanism of the crystallization process, notably differentiating between surface and bulk crystallization.

It is possible to deduce nucleation rates by applying classical nucleation theory from the ERH values recorded from a large enough number of crystallization events. Parsons *et al.*[140] used the ERH from 55 crystallization events of aqueous AS particles levitated in an EDB to deduce a homogeneous nucleation rate, J_{hom}, per unit volume and time, assuming that the nucleation process occurred in the volume of the particles (Fig. 4(a)). Fig. 4(b) shows the logarithm of J_{hom} as a function of $T^{-3}(\ln S)^{-2}$, where S stands for supersaturation given by the ratio of the activity of the solute in solution over the activity of the solute in the saturated solution. A linear relationship between the logarithm of J_{hom} and $T^{-3}(\ln S)^{-2}$ was obtained when crystallization events occurring above ~37% RH were not included in the analysis. This allows speculation that ERH > 37% RH cannot be attributed to a homogeneous nucleation process in the volume of the solution, but might occur on foreign surfaces by heterogeneous nucleation. Similarly, Pant *et al.*[39] used optical microscope observations of efflorescence occurring on droplets deposited on a hydrophobic substrate to deduce a homogeneous nucleation rate of crystalline AS from aqueous solutions. To obtain a linear relationship between the natural logarithm of the nucleation rate ($\ln(J)$) and $(\ln(S))^{-2}$, they also had to neglect efflorescence points > 37.7% RH.

Ciobanu *et al.*[142] investigated the efflorescence of aqueous AS droplets deposited on a hydrophobically coated substrate with a high speed camera and compared these results with efflorescence occurring in aqueous AS droplets with a poly(ethylene glycol)-400 (PEG-400) coating. Interestingly, efflorescence of the coated droplets happened at 24–34% RH which is distinctly lower than the values obtained for the pure aqueous AS droplets. From this finding and the evaluation of the location of first crystal growth within the particles, they speculate that volume based nucleation only becomes important below 34%RH and can only be observed when nucleation at the surface of the particle is turned off, *e.g.* by replacing the air/AS solution interface by a PEG-400/AS solution interface.

Letovicite, ammonium bisulphate. Atmospheric aerosols are often acidic. Such acidic aerosols have a larger tendency to remain as a liquid droplet in the atmosphere. Depending on the ammonia to sulphate ratio, the crystallizing solid may be letovicite or ammonium bisulphate (ABS), as can be seen from

Table 1 Full DRH and ERH of single particles consisting of inorganic salts and mixtures of inorganic salts with organic substances. Abbreviations: EDB, electrodynamic balance; Mic, optical microscopy of deposited particles; AS, ammonium sulfate; letov, letovicite; ABS, ammonium bisulfate; AN, ammonium nitrate; n/a, not available, n.o., not observed; M5, malic + malonic + maleic + glutaric + methylsuccinic acid mixture; C5, glutaric + methylsuccinic + dimethylmalonic acid mixture; C6, 2-methylglutaric + 3-methylglutaric + 2,2-dimethylsuccinic acid mixture; C7, 3-methyladipic acid + 3,3-dimethylglutaric acid + diethylmalonic acid mixture. The asterix in the reference column indicates that also hygroscopic growth data is available. In the T column, 'RT' means room temperature and we use 'RT(?)' if the authors do not state the temperature explicitly but room temperature is most likely to apply

Technique	Inorganic salt	Organic substance	Mixing ratio Inorg:org	Full DRH	ERH	T	Ref.
EDB	AS	—	—	80–81	37–48	293 K, RT	138 (ref. 51, 71, 74)
EDB	AS	—	—	80.1–80.5	45.4–45.6	RT	139
Mic	AS	—	—	n/a	34.3–42.5	293 K	39
EDB	AS	—	—	n/a	34–39	295–300 K	140
Mic	AS	—	—	n/a	37.5–40	295–297 K	141*
Mic	AS	—	—	n/a	36–44	293 K	142
EDB	AS	Malonic acid	1 : 1 (mole)	73.7	45.9–46.9	RT	143*
EDB	AS	Malonic acid	1 : 1 (mole)	75–79	16–20	RT	144
Mic	AS	Malonic acid	88 : 12 (mole)	~80	31–35	293 K	145
Mic	AS	Malonic acid	76 : 24 (mole)	~78	28–31	293 K	145
Mic	AS	Malonic acid	64 : 36 (mole)	~76	0–23	293 K	145
Mic	AS	Malonic acid	47 : 53 (mole)	~72.5	n.o.	293 K	145
EDB	AS	Malonic acid	76 : 24 (mole)	n/a	27–38	295–300 K	140
EDB	AS	Malonic acid	64 : 36 (mole)	n/a	15–34	295–300 K	140
EDB	AS	Malonic acid	47 : 53 (mole)	n/a	0–18	295–300 K	140
Mic	AS	Malonic acid	1 : 1 (mole)	~74	Incomplete	RT	146*
EDB/Mic	AS	Malonic acid	9 : 1 (mole)	~79	n/a	RT(?)	147
EDB/Mic	AS	Malonic acid	4 : 1 (mole)	~78.5	n/a	RT(?)	147
EDB/Mic	AS	Malonic acid	7 : 3 (mole)	~78	n/a	RT(?)	147
EDB/Mic	AS	Malonic acid	3 : 2 (mole)	~77	n/a	RT(?)	147
EDB/Mic	AS	Malonic acid	1 : 1 (mole)	~74	n/a	RT(?)	147
EDB/Mic	AS	Malonic acid	2 : 3 (mole)	~74	n/a	RT(?)	147
EDB/Mic	AS	Malonic acid	3 : 7 (mole)	~71	n/a	RT(?)	147
EDB	AS	Succinic acid	1 : 1 (mole)	79.0	48.3	RT	143*
EDB	AS	Succinic acid	1 : 1 (mole)	~80	~30	RT	144*
EDB	AS	Glutaric acid	1 : 1 (mole)	76.6	55.7–59.2	RT	143*
EDB	AS	Glutaric acid	87 : 13 (mass)	80.7–81.1	50.3–51.0	RT	139*
EDB	AS	Glutaric acid	51 : 49 (mass)	79.0–80.9	40.6–40.9	RT	139*
EDB	AS	Glutaric acid	1 : 1 (mole)	78–80	31–36	RT	144*
Mic	AS	Glutaric acid	9 : 1 (mole)	~79.5	~34	293 K	148
Mic	AS	Glutaric acid	4 : 1 (mole)	~79	~34	293 K	148
Mic	AS	Glutaric acid	7 : 3 (mole)	~79	~33	293 K	148
Mic	AS	Glutaric acid	3 : 2 (mole)	~79.5	~32.5	293 K	148
Mic	AS	Glutaric acid	1 : 1 (mole)	~79	~29.5	293 K	148
EDB	AS	Glutaric acid	1 : 1 (mole)	80.9	40	RT	25*
EDB	AS	Glutaric acid	9 : 1 (mass)	~78	n/a	297 K	149
EDB	AS	Glutaric acid	4 : 1 (mass)	~78	n/a	297 K	149
EDB	AS	Glutaric acid	7 : 3 (mass)	~79	n/a	297 K	149
EDB	AS	Glutaric acid	7 : 3 (mass)	~79	n/a	288 K	149
EDB	AS	Glutaric acid	7 : 3 (mass)	~79.5	n/a	283 K	149
EDB	AS	Glutaric acid	3 : 2 (mass)	~77	n/a	297 K	149
EDB	AS	Glutaric acid	1 : 1 (mass)	~78	n/a	297 K	149
EDB	AS	Glutaric acid	1 : 1 (mass)	~78	n/a	288 K	149
EDB	AS	Glutaric acid	1 : 1 (mass)	~79	n/a	283 K	149
EDB/Mic	AS	Glutaric acid	9 : 1 (mole)	~78	n/a	RT(?)	147
EDB/Mic	AS	Glutaric acid	4 : 1 (mole)	~78	n/a	RT(?)	147
EDB/Mic	AS	Glutaric acid	7 : 3 (mole)	~79	n/a	RT(?)	147
EDB/Mic	AS	Glutaric acid	3 : 2 (mole)	~77	n/a	RT(?)	147
EDB/Mic	AS	Glutaric acid	1 : 1 (mole)	~78	n/a	RT(?)	147
EDB	AS	Glutaric acid	1 : 1 (mole)	~77.5	~32	290–291 K	150*
Mic	AS	Glutaric acid	1 : 1 (mole)	78.5	32.5–36	RT	146*
EDB	AS	Adipic acid	1 : 1 (mass)	~80	n/a	290 K	151*
EDB	AS	Adipic acid	1 : 2 (mass)	~80	n/a	290 K	151*
EDB	AS	Adipic acid	1 : 3 (mass)	78–83	n/a	290 K	151*
EDB	AS	Adipic acid	2 : 1.1 (mole)	~79	~38	290–291 K	150*
EDB	AS	Adipic acid	1 : 3.3 (mole)	~80	~35	290–291 K	150*
Mic	AS	Adipic acid	97 : 3 (mass)	80	34–40	RT	141
Mic	AS	Adipic acid	9 : 1 (mass)	79	31–39.5	RT	141*
Mic	AS	Adipic acid	4 : 1 (mass)	80	34–42	RT	141
Mic	AS	Adipic acid	7 : 3 (mass)	80	39–42	RT	141*
Mic	AS	Adipic acid	1 : 1 (mass)	80	34–42	RT	141*
Mic	AS	Adipic acid	3 : 7 (mass)	81	33–39.5	RT	141
Mic	AS	Adipic acid	1 : 9 (mass)	80.5	37	RT	141
EDB	AS	Adipic acid	97 : 3 (mass)	~80	34	RT	141*
EDB	AS	Adipic acid	9 : 1 (mass)	~80	34	RT	141*

Table 1 (*continued*)

Technique	Inorganic salt	Organic substance	Mixing ratio Inorg:org	Full DRH	ERH	T	Ref.
EDB	AS	Citric acid	1 : 1 (mole)	n/a	n/a	RT	143*
EDB	AS	Citric acid	4 : 1 (mole)	~80	~38	290–291 K	150*
EDB	AS	Citric acid	2 : 1 (mole)	~76	n.o.	290–291 K	150*
EDB	AS	Citric acid	1 : 1 (mole)	n.o.	n.o.	290–291 K	150*
EDB	AS	Maleic acid	9 : 1 (mass)	~80	n/a	297 K	149
EDB	AS	Maleic acid	4 : 1 (mass)	~79	n/a	297 K	149
EDB	AS	Maleic acid	7 : 3 (mass)	~76	n/a	297 K	149
EDB	AS	Maleic acid	7 : 3 (mass)	~77.5	n/a	288 K	149
EDB	AS	Maleic acid	7 : 3 (mass)	~79	n/a	283 K	149
EDB	AS	Maleic acid	3 : 2 (mass)	~73	n/a	297 K	149
EDB	AS	Maleic acid	1 : 1 (mass)	~70	n/a	297 K	149
EDB	AS	Maleic acid	1 : 1 (mass)	~74	n/a	288 K	149
EDB	AS	Maleic acid	1 : 1 (mass)	~75	n/a	283 K	149
EDB/Mic	AS	Maleic acid	91 : 1 (mole)	~80	n/a	RT(?)	147
EDB/Mic	AS	Maleic acid	82 : 18 (mole)	~78	n/a	RT(?)	147
EDB/Mic	AS	Maleic acid	73 : 27 (mole)	~76	n/a	RT(?)	147
EDB/Mic	AS	Maleic acid	64 : 36 (mole)	~74	n/a	RT(?)	147
EDB/Mic	AS	Maleic acid	56 : 44 (mole)	~71	n/a	RT(?)	147
EDB	AS	Tartaric acid	n/a	n.o.[a]	n.o.[a]	n/a	149
EDB	AS	M5	1 : 1 (mass)	73.3	26–28	290 K	6*
EDB	AS	M5	4 : 1 (mass)	78.3	35	290 K	6*
Mic	AS	C5	4 : 1 (mass)	77.8	40.8	293 K	41
Mic	AS	C5	1 : 1 (mass)	77.5	37.9	293 K	41
Mic	AS	C5	1 : 2 (mass)	75.1	32.4	293 K	41
Mic	AS	C6	12 : 1–1 : 1 (mass)	77–80	41–46	293 K	41
Mic	AS	C6	1 : 2–1 : 4 (mass)	76–80	36–48	293 K	41
Mic	AS	C6	1 : 5–1 : 12 (mass)	71–76	30–40	293 K	41
Mic	AS	C7	12 : 1–1 : 1 (mass)	78–81	40–48	293 K	41
Mic	AS	C7	1 : 2–1 : 8 (mass)	78–80	38–43	293 K	41
Mic	AS	C7	1 : 10–1 : 23 (mass)	74–76	37–40	293 K	41
Mic	AS	C7	1 : 41 (mass)	70.1	33.5	293 K	41
EDB	AS	Suwannee River Fulvic Acid	1 : 1 (mass)	79.8–82.5	39.8–43.6	RT	152*
Mic	AS	Suwannee River Fulvic Acid	9 : 1 (mass)	~80.5	n/a	293 K	145
Mic	AS	Suwannee River Fulvic Acid	4 : 1 (mass)	~80	n/a	293 K	145
Mic	AS	Suwannee River Fulvic Acid	2 : 1 (mass)	~80	n/a	293 K	145
Mic	AS	Suwannee River Fulvic Acid	48 : 52 (mass)	~79	n/a	293 K	145
EDB	AS	Nordic Aquatic Fulvic Acid	1 : 1 (mass)	78.6–81.4	38.1–41.5	RT	152*
EDB	AS	Octanoic acid	91 : 9 (mass)	80.5–81.2	45.3–45.6	RT	153*
EDB	AS	Octanoic acid	66 : 34 (mass)	82.7–83.2	41.0–41.6	RT	153*
EDB	AS	Octanoic acid	18 : 82 (mass)	79.6–81.6	41.5–44.2	RT	153
EDB	AS	Octanoic acid	30 : 70 (mass)	78.5–81.8	42.2–45.1	RT	153
EDB	AS	Glycerol	1 : 1 (mole)	77.8	28.2	RT	143*
Mic	AS	Glycerol	88 : 12 (mole)	~80	22–33	293 K	145
Mic	AS	Glycerol	77 : 23 (mole)	~78	19–30	293 K	145
Mic	AS	Glycerol	63 : 37 (mole)	~77	0–24	293 K	145
Mic	AS	Glycerol	1 : 1 (mole)	~74	0–14	293 K	145
Mic	AS	Glycerol	42 : 58 (mole)	~72	0–8	293 K	154
Mic	AS	Levoglucosan	86 : 14 (mole)	~80	28–32	293 K	154
Mic	AS	Levoglucosan	3 : 1 (mole)	~78	24–28	293 K	154
Mic	AS	Levoglucosan	61 : 39 (mole)	~75	16–22	293 K	154
Mic	AS	Levoglucosan	44 : 56 (mole)	~72	8–17	293 K	154
EDB	AS	Levoglucosan	1 : 1 (mole)	n.o.	n.o.	RT	155,156*
EDB	AS	PEG-400	1 : 1 (mass)	80–82	33–37	290 K	6*
Mic	AS	PEG-400	8 : 1–1 : 8 (mass)	~80	24–43	293 K	43
Mic	AS	PEG-400	1 : 1 (mass)	~80	26.8–33.9	293 K	142
Mic	AS	PEG-400	1 : 8 (mass)	~80	24.3–29.3	293 K	142
EDB	Letov	—		69	35	RT	138 (ref. 51, 81)
EDB	Letov	—		72.8 ± 2.5	27.5 ± 2.5	263.5 K	22*
EDB	Letov	Malonic acid	83 : 17 (mole)	n/a	23–27	RT	140
EDB	Letov	Malonic acid	64 : 36 (mole)	n/a	5–13	RT	140
EDB	Letov	Malonic acid	48 : 52 (mole)	n/a	0–16	RT	140
EDB	ABS	—		39–40		RT	138 (ref. 51, 81)
	ABS	—		66–76[b]	16 ± 2.5[b]	260–270 K	22
EDB	ABS	Malonic acid	83 : 17 64 : 36 48 : 52 (mole)	n/a	n.o.	RT	140
EDB	ABS	Levoglucosan	1 : 1 (mole)	n.o.	n.o.	RT	155,156
EDB	NaCl	—	—	72–77	39–54	RT	157and refs therein
Mic	NaCl	—	—	~75	46–48	293 K	148
EDB	NaCl	—	—	75 ± 1	44–46	293 K, RT	138 (ref. 50, 71, 74)
EDB	NaCl	Malonic acid	1 : 1 (mole)	65.8	50.8–52.4	RT	143*

Table 1 (*continued*)

Technique	Inorganic salt	Organic substance	Mixing ratio Inorg:org	Full DRH	ERH	T	Ref.
EDB	NaCl	Malonic acid	1 : 1 (mole)	67 ± 1	~31%	295 K	158*
EDB	NaCl	Succinic acid	1 : 1 (mole)	72.8	53.2–53.4	RT	143*
EDB	NaCl	Glutaric acid	1 : 1 (mole)	70.7	54.4	RT	143*
Mic	NaCl	Glutaric acid	9 : 1 (mole)	~75	n/a	293 K	148
Mic	NaCl	Glutaric acid	4 : 1 (mole)	~74	45–49	293 K	148
Mic	NaCl	Glutaric acid	7 : 3 (mole)	~74	45–47	293 K	148
EDB	NaCl	Glutaric acid	2.4 : 1 (mole)	>75	30–40	295 K	158
EDB	NaCl	Citric acid	1 : 1 (mole)	62.3	38.2–41.8	RT	143*
EDB	NaCl	Octanoic acid	Coating	~75	n/a	RT	159
EDB	NaCl	Suwannee River Fulvic Acid	1 : 1 (mass)	74.2–76.8	47.1–50.2	RT	152*
EDB	NaCl	Nordic Aquatic Fulvic Acid	1 : 1 (mass)	74.8–77.4	49.5–52.6	RT	152*
EDB	NaCl	Glycerol	1 : 1 (mole)	72.7	38.9	RT	143*
EDB	NaCl	Tween 80	5 : 1 (mole)	72–73	~54–57	20–25 °C	157*
EDB	NaCl	Tween 80	3 : 1 (mole)	70–72	~48–53	20–25 °C	157*
EDB	AN	—	—	61.8 ± 0.3	n.o.	RT	160*
Mic	AN	—	—	~62	0–30	RT	146*
EDB	AN	Succinic acid	7 : 1 (mass)	61.4 ± 0.4	42.6 ± 1.8[c]	RT	160*
EDB	AN	Succinic acid	3 : 1 (mass)	61.0 ± 0.3	44.3 ± 0.7[c]	RT	160*
EDB	AN	Succinic acid	1 : 1 (mass)	60.6 ± 0.4	44.8 ± 0.8[c]	RT	160*
EDB	AN	Levoglucosan	1 : 1 (mole)	n.o.	n.o.	RT	155,156*

[a] poorly soluble ammonium tartrate presumably formed. [b] letovicite formed. [c] heterogeneous nucleation on succinic acid.

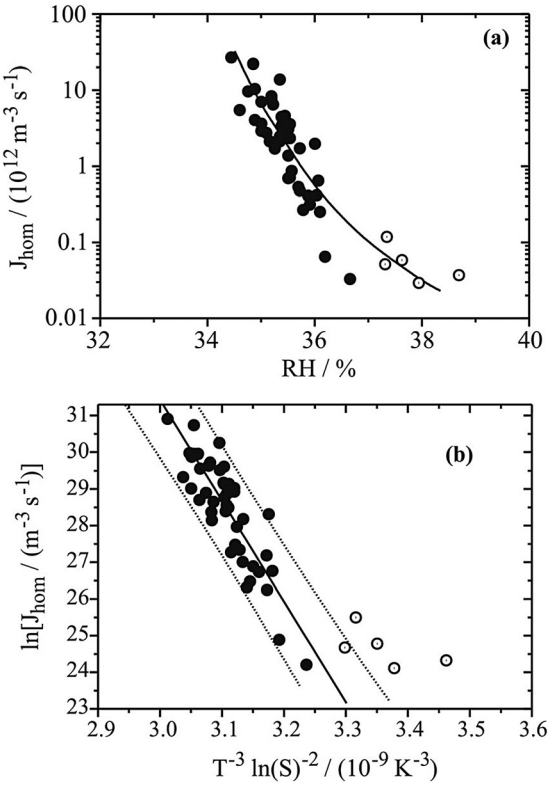

Fig. 4 (a) Homogeneous nucleation rate, J_{hom}, as a function of RH for $(NH_4)_2SO_4$. The number of particles remaining completely liquid as a function of RH was measured in an EDB to derive the rate. The line is to guide the eye only. The 10% nucleation events occurring at highest RH are singled out as open symbols. (b) Classical nucleation theory predicts an exponential dependence of the rate with inverse supersaturation squared. The solid line is a fit through all but the 10% nucleation events which occurred at highest RH (open symbols), the dashed lines indicate the 95% prediction band. The nucleation events singled out as open symbols might be influenced by heterogeneous nucleation. [Adapted with permission from ref. 140, Copyright 2006 American Chemical Society.]

water-sulfuric acid-AS phase diagrams.[161,162] However, the thermodynamic stable phase is not necessarily the one that crystallizes. Single particle studies are able to determine the nature of the crystallized phase *e.g.* by Raman spectroscopy. Using this technique, Colberg *et al.*[22] showed that letovicite crystallized for a single particle levitated in the EDB with an ammonia to sulphate ratio of 1 : 1.

Sodium chloride. Table 1 includes a selection of DRH and ERH values that have been measured on single particles of NaCl. NaCl is often used to calibrate RH sensors mounted in single particle instruments because its DRH is accurately known to be 75.3% at 25 °C (*e.g.* ref. 163). The spread of NaCl DRHs therefore reflects the accuracy of the instruments. The scatter of ERH, on the other hand reflects the stochastic nature of the nucleation process. Nucleation rates (s^{-1}) increase with droplet size leading to higher ERH for larger droplets. Moreover some of the highest observed ERH might be caused by heterogeneous nucleation when solid impurities are present in the droplets.

Ammonium nitrate. Ammonium nitrate (AN) deliquesces at ~62%RH. Upon drying, some particles show efflorescence while others remain as supersaturated solutions down to the lowest RH that can be reached. These contradictory results have been discussed in detail by Lightstone *et al.*[160] They speculate that some studies may have been hampered by the presence of impurities that limited the degree of supersaturation that could be achieved. One complication of AN is that its components, NH_3 and HNO_3, have a sufficiently high vapour pressure to make solute evaporation significant on the timescales of typical single particle measurements. This partial evaporation changes the NH_3 : HNO_3 stoichiometry and might influence nucleation.

Organic substances. Organic substances have been investigated extensively in EDB and microscopy experiments. Among the substance classes that have been investigated are di- and polycarboxylic acids,[164] dicarboxylic salts,[154,165] humic acids,[166]

sugars,[167,168] polyols,[169,170] amino acids,[10,171] and anhydrosugars.[10,155] A compilation of literature with water activity data can be found in Kanakidou *et al.* (Table 7).[172] The organic substances can be divided in two classes depending on their behaviour when exposed to humidity cycles, namely those that show deliquescence and efflorescence and those that show a continuous water uptake and release. As a general rule, substances with a low aqueous solubility, such as succinic acid, tend to effloresce in single particle experiments, while substances with high aqueous solubility, like malonic acid, tend to remain in a supersaturated metastable state even at low RH. These supersaturated solution may reach high viscosities at low RH or even turn glassy. Zobrist *et al.*[49] showed that a sucrose crystal that had been injected into an EDB deliquesced at 85.6%RH upon humidification, but then turned into a glass on drying instead of crystallising. The kinetic limitations imposed on achieving equilibrium in highly viscous and glassy aerosol are discussed more in section Vb.

The organic aerosol fraction is always present as a complex mixture of a high number of mostly oxygenated hydrocarbons (*e.g.* ref. 172). Marcolli *et al.*[7] and Marcolli and Krieger[6] have shown for a mixture of five dicarboxylic acids (M5) that DRH of the mixture is lowered compared to DRH of the single components and that the particle remains as a supersaturated solution in the EDB. This depression of DRH results from the entropy change of mixing when a high number of components are mixed together. To mimic the organic fraction in the atmosphere, organic substances or organic mixtures that do not show efflorescence and deliquescence are therefore most appropriate.

Mixed organic/inorganic particles. Single particle measurements on atmospheric aerosol have shown that the oxygenated organic aerosol fraction is internally mixed with the inorganic salts (*e.g.* ref. 173, 174). Because of the strong depression of DRH and ERH of minor components in mixtures, we do not expect efflorescence of the organic compounds to occur. However, a question arises: what is the influence of the organic fraction on DRH and ERH of the inorganic salts? Table 1 gives an overview of the studies that investigated deliquescence and efflorescence of single particles consisting of organic/inorganic mixtures. This table excludes HTDMA studies, which are performed on an ensemble of particles and not on a single particle that is monitored over a longer period of time. Summaries of HTDMA measurements can be found in Chan and Chan[175] or Kanakidou *et al.*[172] Among the salts that have been chosen for such studies there is a strong predominance of AS followed by NaCl. Only a few studies have investigated AN, letovicite and ABS. On the organic side, dicarboxylic acids are the most common representatives. Table 1 shows that in mixtures with NaCl, the highly hydrophilic citric and malonic acids exert the largest depression of DRH and ERH, while the fulvic acids have virtually no effect. Mixtures with AS show a similar picture: the largest depressions of DRH and ERH are observed for the most hydrophilic dicarboxylic acids, while again the fulvic acids leave the DRH and ERH unchanged. A depression of DRH occurs when the solubility of the salt per mass of water is increased by the addition of an organic substance. If the presence of organics decreases the solubility of the inorganic salt, DRH remains virtually unchanged and a liquid–liquid phase separation may occur (*e.g.* Marcolli and Krieger[6] and Zuend *et al.*[17]). ERH depends on the solubility of the salt in the presence of the organics in a similar way as DRH. In addition to this thermodynamic effect, ERH is also influenced by kinetic factors (*e.g.* viscosity of the solution) and can show both an increase or a decrease with respect to the value in pure aqueous solutions.

Some organic substances like citric and malonic acid or glycerol may prohibit crystallization of AS totally. Most of the mixtures investigated were dominated by the inorganic salt component with the organic substance as the minor component. Frequently 1 : 1 mixtures (mole or mass ratio) have been investigated. If the organic fraction were increased even further, much stronger reductions of DRH and total prevention of ERH should be expected, although this composition range has received very little attention. Bertram *et al.*[21] have used these single particle studies together with other deliquescence and efflorescence data to parameterize ERH and DRH of mixed particles of AS and organics using the organic-to-sulfate mass ratio of the particle and the oxygen-to-carbon elemental ratio of the organic component.

III.b Hygroscopic growth

In addition to Table 1 summarising DRH and ERH values recorded for a wide range of compounds, the studies which have reported measurements of hygroscopic growth have also been indicated. EDB measurements can allow the mass or volume change of single particles during humidity cycles to be accurately determined; in addition, optical tweezers can be used to investigate hygroscopic growth with very high accuracy. Most growth measurements are limited by the accuracy with which the RH can be measured, typically of the order of $\pm 1\%$. For a hygroscopic component such as sodium chloride, the growth factor changes by $\sim 0.5\%$ per% RH change at a RH of $\sim 50\%$, rising to $\sim 5\%$ per% RH change at 95%. Thus, inaccuracies in the measurement of RH of $\pm 1\%$ can lead to growth factors that are 5% higher or lower than their true values. The improvement to this level of accuracy that can be achieved in comparative optical tweezers measurements is described below.

Assuming that the mass or volume change can be fully attributed to water uptake or release accompanying an RH change, water activity a_w can be determined as a function of water content of the aqueous solution if the particle is in equilibrium with the surrounding gas phase, *i.e.* if a_w equals RH. Such data are unique because single particles persist as aqueous solution droplets up to high supersaturation that cannot be reached by bulk measurements. This concentration range is important for examining the hygroscopic growth of aerosol particles and is particularly important for quantifying their impact on the direct aerosol effect.

Water activity data of supersaturated solutions are needed for the accurate parameterization of thermodynamic activity coefficient models such as E-AIM (Extended Aerosol Inorganics Model), website: http://www.aim.env.uea.ac.uk/aim/aim.php,[176,177] and AIOMFAC (Aerosol Inorganic–Organic Mixtures Functional groups Activity Coefficients), website: http://www.aiomfac.caltech.edu/index.html,[155,178] which aim at covering the whole composition

range that occurs in atmospheric aerosol particles. For this purpose, a high level of accuracy is required for the single particle techniques to really contribute. In addition to an accurate RH measurement, accurate mass, size or refractive index determinations are also essential.

A reference concentration is required for the determination of solute concentration in EDB measurements from measurements of the relative particle mass, a consequence of the fact that absolute particle masses cannot be easily determined. Usually EDB data are represented as mass growth factors: $g_m(RH) = m(RH)/m_0$. Typically one of two approaches is used to provide the reference mass, m_0: either the reference mass is assumed to be proportional to the voltage recorded for levitating a dry particle at $< 5\%$ RH or a droplet at low concentration and high RH, for which bulk water activity data are available, is chosen. Although the former has been mostly used, we recommend that the latter provides a more robust reference, since a dry particle may retain some water or may not be in thermodynamic equilibrium (see section V). In optical tweezers measurements, the diameter growth factor is determined: $g_d(RH) = D(RH)/D_0$. The composition at a high reference RH at which the solution droplet can be assumed to be homogeneous is used to estimate an equivalent dry particle diameter, D_0. To calculate concentration from size data, the density of the solution is needed and this is often estimated from volume additivity mixing rules. The refractive index data can be used to infer concentration as well, if reference bulk data are available.

Hygroscopic growth data cannot be derived accurately from the diameter change of droplets deposited on a hydrophobic substrate because the contact angle between the droplet and the substrate changes by an unknown amount during a humidity cycle.[43] As an alternative, peak intensities of water and solute peaks in micro-Raman spectra taken from the droplets can be quantified to derive hygroscopic growth, as was shown *e.g.* by Yeung *et al.*[141] and Yeung and Chan.[146]

For many inorganic salts including AS, ABS, letovicite, NaCl and AN the hygroscopic growth of single particles during humidity cycles in EDB experiments has been accurately parameterized by Tang and Munkelwitz[106] and Tang.[179] Fig. 5 gives an example of such measurements: panel (a) shows a hygroscopicity cycle of AS with EDB mass data from Zardini *et al.*,[150] Clegg *et al.*,[180] Tang and Munkelwitz,[181] and model calculations from AIOMFAC and E-AIM. Panel (c) shows the hygroscopic cycle of citric acid (CA) with EDB mass data from Zardini *et al.*[150] and Peng *et al.*,[164] compared with model predictions of AIOMFAC. Panel (b) shows a hygroscopic cycle of a 1 : 1 (molar or mass) ratio mixture of CA and AS with experimental data from Zardini *et al.*,[150] and Choi and Chan[143] together with Zdanovskii-Stokes-Robinson (ZSR) and AIOMFAC model predictions. The ZSR relation assumes independent (*i.e.* linearly additive) hygroscopic behaviour of the different components in a mixed particle.[182–184] The accuracy of this type of measurements is limited by the accuracy of the RH sensor and, to some extent, by drifts and feedback accuracy of the mass measurements in the EDB. In case accurate density and refractive index data are available, converting radius measurements using elastic light scattering to mass growth may yield more accurate hygroscopic growth curves than evaluation of the DC voltage.[151]

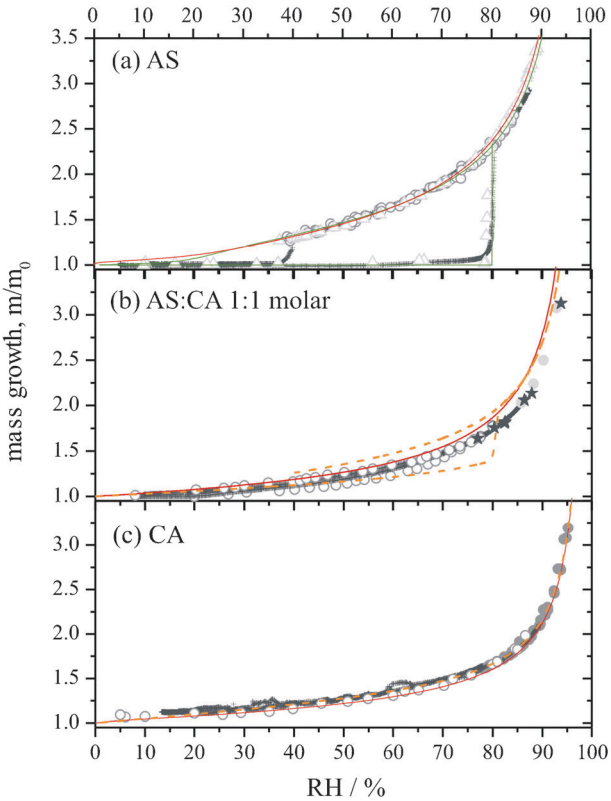

Fig. 5 Hygroscopic growth measured in EDB experiments compared to thermodynamic modelling: (a) AS (black crosses, ref. 150; open triangles, ref. 106; open circles,ref. 180; green line E-AIM, red line AIOMFAC); (b) mixture of AS and citric acid 1 : 1 molar (black crosses EDB, filled stars bulk,[150] open circles EDB, filled circles bulk,[143] red line AIOMFAC, orange dashed line ZSR[150]); (c) citric acid (black crosses, ref. 150; open circles EDB, closed circles bulk, ref. 164; red line AIOMFAC).

Optical tweezers measurements on single trapped solution droplets can allow the variation in diameter growth factor with RH to be determined in an analogous way to EDB measurements.[48,121,185] The appearance of WGMs in the Raman band can be used to accurately determine the size and refractive index of the trapped solution droplet and the change in size with RH can be measured. When trapping dilute solution droplets at very high RH ($>95\%$) from a mist generated by a medical nebuliser, it has been shown that the droplet composition immediately when captured can be assumed to be the same as that of the nebulised solution.[186] However, at such high RH, the accuracy of capacitance type probes is questionable. A much more accurate way of determining the local RH in the trapping environment to map out the growth curve for the aerosol is to use a second droplet of known hygroscopic response, usually aqueous sodium chloride.[186,187] As the size of this second control droplet varies, the local RH can be inferred with an accuracy estimated to be better than $\pm 0.09\%$ and with sub-second time-resolution. In effect, the hygroscopic growth of two particles can be studied in a comparative way and measurements have been made on up to five droplets at the same time using holographic optical tweezing to capture an array of droplets.[93]

The comparative approach has been used to investigate the hygroscopic growth of mixed component aerosol, such as

mixtures of ammonium sulphate or sodium chloride with a dicarboxylic acid such as glutaric acid.[187] From such measurements, it was shown that the maximum difference between the measured wet particle size and that predicted from the Aerosol Diameter Dependent Equilibrium Model (ADDEM) was < 1% or at most 30 nm for a 4 μm radius NaCl-glutaric acid solution droplet. Indeed, many of the measurement radii were ≪1% from the predictions and corresponded to only a few nanometers error in size on a droplet > 3 μm in radius above 96% RH. The ADDEM model uses the same thermodynamic parameterisations as E-AIM and treats the density of the mixed component solution by a volume additivity approach.[188]

Using optical landscapes to control aerosol flow and to load chemically distinct droplets into different traps, Walker *et al.* have shown that the hygroscopic response of an ammonium sulphate droplet can be compared with a sodium chloride droplet; examples of the accuracy of the growth measurements that can be made is shown in Fig. 6.[189] Indeed, the uncertainties

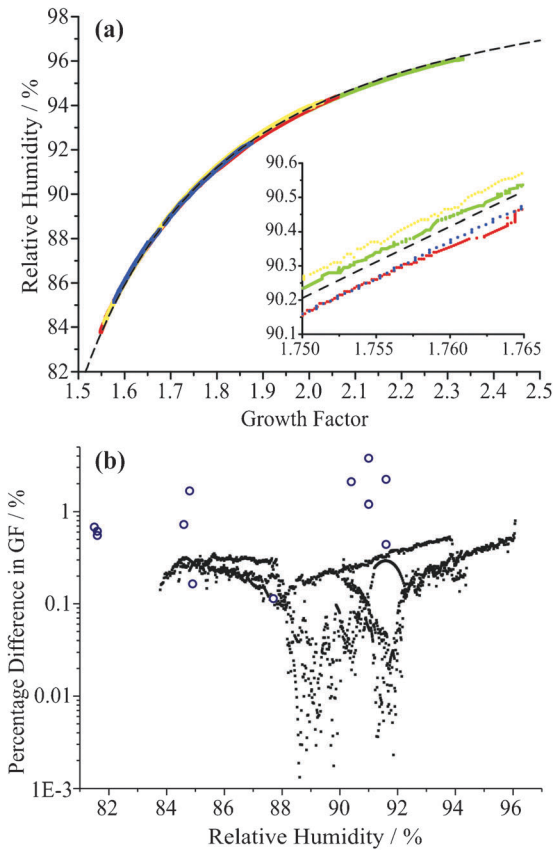

Fig. 6 (a) The dependence of the growth factor of ammonium sulphate aerosol on RH measured using optical tweezers. The RH is determined from a second trapped droplet of sodium chloride. Data are shown for four measurements in different colours. The predicted growth factors from the ADDEM model are shown by the dashed line. The inset shows the typical variation between measurements and the level of agreement with the model predictions. (b) Percentage difference between GFs measured and calculated from ADDEM model for AS aerosol: Small black symbols, comparative tweezers measurements for AS; open blue circles, tweezers measurements of AS equilibrium size with RH determined by a capacitance probe instead of a control droplet. [Adapted with permission from ref. 189, Copyright 2010 American Chemical Society.]

associated with these comparative measurements are considerably lower than achieved from more conventional measurements on single droplets with differences between measurements and model predictions mostly less than 0.1% in diameter growth factor between 80 and 95% RH, an error at the nanometre level for droplets 4 μm in radius. This allows substantive validation of thermodynamic models with high accuracy up to water activities relevant to the activation of CCN. Notably, this level of accuracy in the measured growth factors (better than 0.1%) is considerably better than the errors achieved with conventional RH probes, which are typically at the ±5% level at 95% RH, as discussed above.

III.c Liquid–liquid phase separation

Liquid–liquid phase separation (LLPS) occurs when compounds of very different polarity are mixed together. If significant amounts of non-polar compounds from, *e.g.*, primary anthropogenic emissions are mixed together with components that are mostly oxygenated secondary organic aerosol, LLPS is expected over the whole RH range even in the absence of inorganic salts (*e.g.* ref. 190). The tendency of organic solutions to segregate into a separate liquid phase is strongly enhanced by the presence of electrolytes because of the salting-out effect, in which the aqueous solubility of an organic substance is decreased when an electrolyte is added. This type of LLPS depends on the water content of the solution and occurs when the moderating influence of water as the common solvent is reduced. The organic and electrolyte components are therefore freely miscible at high water content and RH and separate when the RH is reduced. Such LLPS was recently postulated to be a common phenomenon in mixed organic/sulphate aerosol particles.[6,21,24,43]

Liquid–liquid equilibria are usually determined in bulk experiments by analysing the composition of the separated phases. Since water activities in both phases are the same under thermodynamic equilibrium, this condition can be used for parameterization of thermodynamic models such as AIOMFAC. Single particle studies offer the possibility to measure LLPS for mixtures under conditions where one or several components are supersaturated. Moreover, they can show whether there are kinetic limitations to LLPS in small volumes and give evidence of the morphology of the phase separated particles.

The first system for which LLPS as a function of RH has been investigated on single particles is PEG-400/AS/H_2O. The phase diagram that has been determined by Marcolli and Krieger[6] on bulk solutions showed an LLPS up to ~90% RH that extends over almost the whole composition range. Single particles of PEG-400/AS/H_2O that were investigated in an EDB did not show any direct evidence of LLPS: the fringe pattern in the phase function and the glare spots of the elastically scattered light were consistent with spherical symmetry. A follow-up study investigating single particles deposited on a hydrophobically coated substrate showed clear evidence of LLPS as shown in Fig. 7 (reproduced from 43). No hysteresis was observed between the RH at which phase separation upon drying occurred and the RH at which the separated phases merged upon moistening and good agreement was found with the phase diagram determined on bulk solutions.

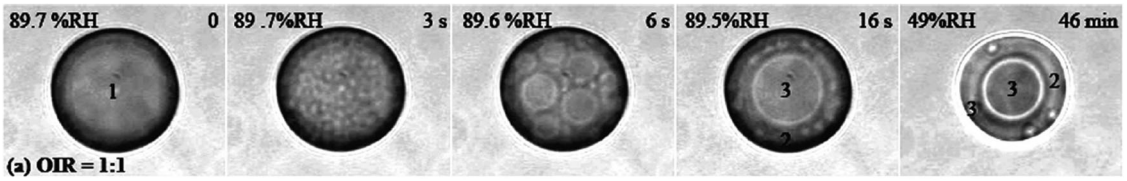

Fig. 7 Liquid–liquid phase separation by spinodal decomposition of a single particle deposited on a hydrophobically coated substrate during a humidity cycle. The particle consists of PEG-400/AS/H_2O with an organic-to-inorganic dry mass ratio OIR = 1 : 1. Small numbers on particle regions indicate composition of phases: 1, aqueous solution of PEG-400 and AS; 2, aqueous PEG-400; 3, aqueous AS. Adapted from Ciobanu *et al.* [Reprinted with permission from ref. 43, Copyright 2009 American Chemical Society.]

We therefore assume that LLPS occurred for the particles levitated in the EDB, but do not have any explanation at present why LLPS did not lead to a distortion of spherical symmetry. Bertram *et al.*[21] detected LLPS in single particles deposited on a hydrophobically coated substrate consisting of AS mixed with organic aerosol model compounds with different oxygen containing functionalities like hydroxyl and carboxylic acid. They related the occurrence of LLPS to the O : C ratio of aerosol particles, postulating O : C <0.7 as condition for LLPS to occur. This finding was confirmed by Song *et al.*[41] who observed dicarboxylic acid/AS/H_2O droplets deposited on a hydrophobically coated substrate with an optical microscope. LLPS occurred for mixtures of dicarboxylic acids with 6 and 7 carbon atoms corresponding to O : C ratios of 0.67 and 0.57, respectively, but not for C5 acids (O : C = 0.8). The study of deposited particles with a Raman microscope seems to be the method of choice for the investigation of liquid–liquid equilibria in mixtures that are supersaturated with respect to the solids of one or several components. Phase diagrams derived from the optically observed phase changes are in good agreement with bulk experiments for systems that have been investigated by both techniques showing that the influence of the substrate/particle interface is too weak to influence thermodynamics. Single particles with LLPS can adopt different morphologies with consequences for heterogeneous and multiphase chemistry, and optical properties. The morphology of single particles consisting of a surfactant, an inorganic salt and water has been studied in detail in optical tweezers experiments (*e.g.* ref. 24,191–193) and will be discussed in detail in the morphology section.

III.d Morphology

The response of aerosol particles to environmental changes does not only depend on their physical state but also on the arrangement of the different phases within the particle, *i.e.* the morphology. Only the phases that partition to the surface of the particle determine accommodation coefficients and heterogeneous nucleation rates. If a particle has a solid or highly viscous coating, the slow diffusion through this coating will determine responses to RH changes or rates of reactions occurring within the particle.

The morphologies of atmospheric aerosol particles that can be conceived when considering surface and interfacial forces that act on the phases present in mixed organic/inorganic particles are summarised schematically in Fig. 1. As discussed above, we expect the organic fraction to be present as a glassy or liquid amorphous phase and the inorganic salt in a crystalline state or dissolved as an aqueous solution. Fig. 8 illustrates the morphologies that should result from combinations of these phases. At low RH the inorganic fraction is most probably crystallized and the organic fraction is in a highly viscous or even glassy state. The morphology resulting from this phase composition is either a crystalline inorganic phase surrounded by a liquid/glassy organic phase (image 1 in Fig. 8) or a crystalline inorganic phase containing the organic phase in veins, pores and cavities (image 2). In a highly viscous organic matrix, the inorganic salt can also be prevented from crystallizing leading to an apparently homogeneous particle which may still show concentration gradients of some components due to slow diffusion (image 3). Over short periods during deliquescence and efflorescence an aqueous organic and an aqueous inorganic liquid phase may coexist with a crystalline inorganic phase. When the inorganic salt is all dissolved, the particle is either present in a one-liquid-phase (image 6) or in a two-liquid-phases state. The conceivable morphologies of particles with two liquid phases are a partially engulfed (image 5) or a core–shell (image 4) configuration.

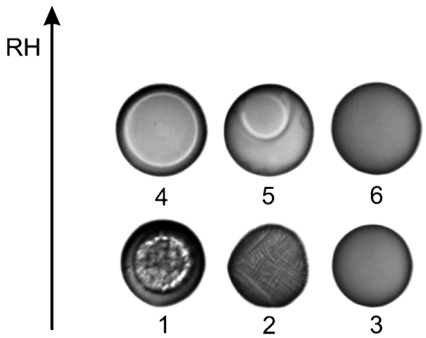

Fig. 8 Optical microscope images of particle morphologies: 1, crystalline phase surrounded by liquid or amorphous phase; 2, crystalline phase containing liquid phase in pores, veins or cavities; 3, mixed liquid or glassy phase, maybe with concentration gradients (cannot be resolved optically); 4, two liquid phases, core–shell configuration; 5, two liquid phases, partially engulfed configuration; 6, mixed liquid phase.

In a core–shell morphology, the phase with the lower surface tension, *i.e.* typically the organic phase, spreads on the aqueous salt phase and totally surrounds it. In a partially engulfed configuration the liquid phases wet each other incompletely and both phases contact the gas phase. Which of these two morphologies is adopted depends on the surface tensions of the aqueous-air and organic-air surfaces and the interfacial tension between the aqueous and organic phases. The estimation of two spreading coefficients is particularly useful in confirming which of these two morphologies is adopted.[24,191]

The spreading coefficient (S_i) of a liquid component (i) spreading over another component (j) can be determined when the surface (σ_{jk}, σ_{ik}) and interfacial (σ_{ij}) tensions are known. The general form of the spreading coefficient, S_i, for two immiscible phases within a third phase k is given by:

$$S_i = \sigma_{jk} - (\sigma_{ij} + \sigma_{ik}) \quad (1)$$

For aerosol, the aqueous phase is designated as phase 1, the organic phase as phase 2 and the gas phase as phase 3. Then, S_1 represents the process of spreading of the aqueous phase on the organic component and this can be assumed to be negative in sign; the spreading of the aqueous phase on the organic phase does not occur spontaneously. The sign of the spreading coefficient for the organic component on the aqueous phase, S_2, can be used to crudely determine the morphology. If S_2 is negative, the organic component does not spread on the surface of the aqueous phase and a partially engulfed structure results with the formation of an organic lens on the aqueous surface; if S_2 is positive, spreading of the organic leads to the formation of a core–shell structure. For systems for which S_2 is close to zero, it is also important to consider the volume ratios of the organic and aqueous phases, with the exact morphology dependent on the relative surface and interfacial areas.[24,191] In addition, knowledge of the surface and interfacial tensions is often poor, particularly for the exact inorganic and organic components of interest.[24] The salting out of organic components to the aqueous surface must be considered, as this lowers the surface energy of the aqueous phase stabilising the formation of partially engulfed structures. However, for many aerosols existing at RHs for which the solutes are supersaturated, bulk measurements of surface and interfacial tensions cannot be made and rationalising the structures of such mixed phase particles relies on extrapolations of bulk data or model predictions of surface tensions at very high solute concentrations.

To determine aerosol particle morphologies experimentally, single particle studies provide the only approach. It is important, however, to remember that the morphology of a particle depends on a subtle balance of surface forces that can be easily biased by additional forces exerted on the particles. A critical assessment of all techniques and their potential pitfalls is needed, preferably by investigating particles of the same composition by all available techniques and comparing the results. This assessment should also include calculations of spreading coefficients using the relationship given in eqn (1) and accurate surface and interfacial tension measurements of the involved phases as input. For all particles smaller than 1 mm in diameter (*i.e.* virtually all atmospheric particles), the influence of gravitational forces on the morphology of mixed phase particles can be safely ignored with capillary forces solely determining particle morphology, as recognised by a Bond number that is $\sim$1 for a mixed hydrophilic and hydrophobic phase droplet for which the aqueous phase has a radius of $\sim$2 mm.[24] By morphology we mean here the contact angles and radii of curvatures of the different surfaces and interfaces. In addition, for sub-micrometer particles we expect that the minor phase is coherent and does not split into multiple inclusions because the former minimizes the interfacial area. For very small inclusions, the Kelvin effect becomes important, further favouring a reduction of the number of inclusions. Moreover, coalescence of multiple phase domains should be fast in such small particles. It should also be realised that although the gravitational force on a particle is not sufficiently strong to distort radii of curvatures of the different phases, it can still determine the relative location of the phases and the predominant location of inclusions which will reside on the underside of a spherical liquid phase for even submicron particles, if its density is higher than the one of the liquid phase.[24] While the influence of optical forces is far too weak to compete with capillary forces for the size of particle investigated by optical tweezers,[194] the influence of surface charge in EDB measurements and the role of the substrate in micro-Raman measurements are less easy to resolve.

Crystallized regions and separate liquid phases can be easily discriminated by optical microscopy as shown in Fig. 8. However, the optical images give only the top view of the particle on the substrate. From this, it is difficult to judge which phases have contact to the droplet/air or the droplet/substrate interface. Moreover, additional forces exerted by the substrate may influence the subtle balance of surface forces and the resulting morphology. Ciobanu *et al.*,[43] Bertram *et al.*,[21] and Song *et al.*[41] have discussed morphologies resulting from LLPS based on optical microscopy and micro-Raman spectroscopy of deposited particles. Ciobanu *et al.*[43] found that PEG-400/AS particles form an inner phase consisting of an aqueous AS solution surrounded by an outer phase consisting of aqueous PEG-400. In addition, the outer phase contained satellite inclusions of aqueous AS. From this, they postulated a core–shell configuration, however, it cannot be excluded that the PEG-400 phase does not spread over the top of the deposited particle.

Bertram *et al.*[21] observed core–shell morphologies with an organic coating surrounding an aqueous ammonium sulphate core for mixtures of AS with different organic substances such as alcohols and organic acids. For some systems, they also observed several sulphate rich inclusions with diameter on the order of a few micrometers within an organic-rich phase. Song *et al.*[41] investigated mixtures of AS with three C6 (2-methylglutaric, 3-methylglutaric, and 2,2-dimethylsuccinic acid) and three C7 (3-methyladipic, 3,3-dimetylglutaric, and diethylmalonic acid) dicarboxylic acids. They observed partially engulfed configuration in the C6/AS/H_2O system for organic-to-inorganic mass ratios OIR = 1 : 1 and 1 : 2 while both partial (OIR = 2 : 1) and complete engulfed (OIR = 1 : 1) configurations occurred in the C7/AS/H_2O system.

In EDB and optical tweezers experiments, analysis of light scattering data can be used to investigate the morphology of particles (Section II). Marcolli and Krieger[6] have not seen a deviation from spherical symmetry for levitated PEG-400/AS particles at relative humidities where two liquid phases are expected to be present. From this, they concluded that the particle adopts core–shell configuration if LLPS indeed occurs, as expected from microscopy and bulk experiments. It remains unclear why a core–shell particle should show undistorted spherical symmetry, because any restoring force keeping the inner phase at the centre of the droplet is expected to be small compared to thermal fluctuations. Therefore, even a completely

wetted inner phase should be located eccentrically in general and hence break the spherical symmetry. Further work is needed to understand the observations and it is particularly important to quantify the ability to resolve between structures that may be very close to spherical from the phase function. If the volume fraction of the organic phase is relatively small compared to the aqueous phase, the composite droplet may still retain spherical symmetry on the lengthscale of the wavelength of the light.

Optical tweezers measurements have been used to examine the morphology of particles containing hydrophilic aqueous and hydrophobic organic liquid domains, providing a further contactless arrangement for interrogating morphology.[24,90,191–193,195] It cannot be ruled out that the gradient force arising from the restoring force acting on the trapped aerosol particle may have an influence on the position of high refractive index inclusions within a mixed phase particle. Some evidence has been reported of the tight confinement of a polystyrene bead (500 nm diameter) within an aqueous droplet, possibly by the action of the trapping beam.[90] However, the optical forces are too small to compete with capillary forces for the sizes of particles studied[194] and observations of morphology are consistent with predictions based on surface and interfacial tensions. The laser power is at all times kept to a minimum, often $\ll$10 mW. The hydrophilic domain has largely contained the inorganic solute sodium chloride; the hydrophobic domain has been decane, octanol or oleic acid. All three examples were shown to form particles that were consistent with partially engulfed morphologies.[24] In all cases, the observations were reconciled with measurements of surface and interfacial tensions. Even in the case of octanol, it was shown that the solubility of octanol in water and the surface excess of octanol residing at the aqueous surface was sufficient to inhibit spreading of the organic component on the aqueous surface: the energy recouped by spreading over the aqueous surface was less than the energy cost for expanding the areas of the organic/water interface and the organic/air surface. For both the decane and oleic acid systems, it was also shown that the morphologies changed in a systematic way with RH. In the former system, the balance of interfacial and surfacial tensions was shown to be such that the S_2 spreading coefficient became positive with decrease in RH, driving a transition from a partially engulfed structure at high RH to a core–shell structure at RHs below $\sim$94%. For the oleic acid system, the extent of the spreading of the organic lens across the aqueous droplet surface was shown to change with RH, illustrating the complex behaviour that can be expected to occur as the aqueous phase volume changes relative to the organic phase with change in RH.[24,61]

A system consisting of crystalline solid and liquid phases that has been investigated in detail by different single particle techniques is adipic acid (AA)/AS/H_2O. Adipic acid is a dicarboxylic acid with a low aqueous solubility (0.15 ± 0.01 mol kg^{-1} water) and a high DRH of 99.9 ± 0.3%.[151] Therefore, when single particles consisting of mixtures of AA and AS are exposed to humidity cycles, AA is expected to remain as crystalline solid that is not involved in water uptake while AS shows deliquescence/efflorescence behaviour. The hygroscopic growth of the mixed particles should hence scale with the AS fraction. Such behaviour was indeed observed by Zardini *et al.*[150] for single particles levitated in an EDB with AS : AA = 2 : 1.1 (molar ratio). However, particles with AS : AA = 1 : 3.3 (molar ratio) showed highly variable pre-deliquescence water uptake of 3–19% in mass starting at RH between 43–53%. For 100 nm diameter particles measured with an HTDMA setup no pre-deliquescence water uptake for AS : AA mass ratios of 1 : 1, 1 : 2, 1 : 3, and 1 : 4 was observed.[151] However, EDB and HTDMA measurements both showed higher water uptake for AS : AA = 1 : 2 and 1 : 3 and a lower one for the 1 : 4 ratio than expected assuming hygroscopic growth only from the AS fraction. Yeung *et al.*[141] observed early water uptake starting at about 70% RH for AS/AA particles with up to 70 wt% AA deposited on a hydrophobic substrate and for particles with 3 wt% and 10 wt% AA levitated in an EDB. This early water uptake was variable from particle to particle and more pronounced in mixtures with lower weight percentages of AA ($<$ 30 wt%). Using Raman spectroscopy, they showed that the pre-deliquescence water uptake is indeed due to partial dissolution of AS, evidenced by the gradual increase in the full width at half height of the sulphate stretching vibration at $\sim$980 cm^{-1}. Sjogren *et al.*[151] and Zardini *et al.*[150] discuss this anomalous water uptake in terms of the complex morphology of the adipic acid matrix possessing veins and pores that enhance water uptake due to an inverse Kelvin effect and enclosures that reduce it because of slow water diffusion through the solid adipic acid. They found evidence for this interpretation by SEM images taken under dry conditions showing that AS/AA mixed particles consisted of a conglomerate of nanocrystals with irregular shapes. Yeung *et al.*[141] confirmed particle heterogeneity on a micrometer scale by comparing AS and AA Raman peak intensities of micro-Raman spectra recorded at different positions on particles deposited on a hydrophobic substrate. Zelenay *et al.*[196] used scanning transmission X-ray microscopy (STXM) and X-ray absorption spectroscopy to monitor morphological changes of submicrometer sized AA/AS particles deposited on a substrate upon water uptake. STXM, which allows imaging with a spatial resolution of 40 nm, confirmed the two phase structure, where adipic acid forms a separate phase of complex morphology partially enclosed by the ammonium sulfate solution at high RH.

The notion of a fine grid of crystals that retains a liquid in pores and veins due to capillary forces was also confirmed by Song *et al.*[41] using micro-Raman spectroscopy of single particles deposited on a hydrophobically coated substrate. Fig. 9 shows Raman spectra of a particle of the C7/AS/H_2O system with OIR = 1 : 1 at 71%RH in the two-liquid-phases state and at 13%RH after efflorescence. AS can be identified by the sharp sulphate stretching vibration at $\sim$975 cm^{-1}, the dicarboxylic acids by a C–H stretching vibration at 2875–2990 cm^{-1}. In the two-liquid-phases state, the phase separation is almost complete, with the inner phase consisting of an aqueous AS solution and the outer phase of an aqueous solution of the dicarboxylic acids. However, in the spectrum of the crystallized particle, AS and dicarboxylic acid peaks appear together showing that domains of both phases coexist at least on a micrometer scale (*i.e.* the spatial resolution of the micro-Raman spectrometer) indicating that the liquid organic outer phase was driven into pores and veins of the crystalline inner phase by capillary forces.

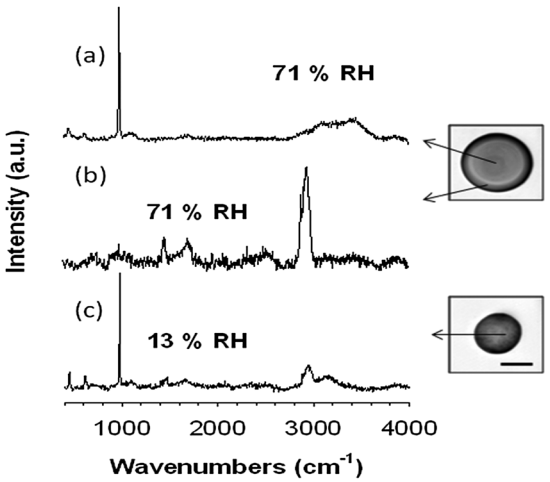

Fig. 9 Raman spectra and microscopic images of a C7/AS/H_2O particle with OIR = 1 : 1 in the two-liquid-phases state (spectra (a) and (b)) and after efflorescence (spectrum (c)). Size bar in the microscopic image: 20 μm. [Reprinted with permission from ref. 41, Song *et al.*]

III.e Polymorphism

Polymorphs are different solid forms of the same chemical compound, which have distinctive properties. In pseudopolymorphism the different crystal forms are hydrates or solvates that contain in addition water or solvent molecules, respectively. Whether a substance exhibits polymorphism or pseudopolymorphism has to be established empirically by cooling or quenching of melts, by condensation of vapour, or by crystallization from solvents under different conditions. There is a fixed order of stability between polymorphic forms, which can be established *e.g.* by measuring their vapour pressures or by determining their saturation solubility. Polymorphs may be in an enantiotropic or monotropic relationship: an enantiotropic relationship implies that each form has a range of temperature over which it is stable with respect to the other and a transition point at which the forms are equistable and in principle interconvertible. In the case of a monotropic relationship, one form is metastable with respect to another at all temperatures.[197]

Standard technique to discriminate between polymorphs are X-ray powder diffraction, which directly probes the crystal lattice, and thermal techniques like differential scanning calorimetry that monitor phase changes as a function of temperature. Spectroscopic techniques like Raman and IR spectroscopy can also be used to distinguish between polymorphic forms since differences in conformations and intermolecular interactions result in peak shifts. Because of the high degree of supersaturation that single particles can attain before solidifying, metastable states often result that cannot be attained in bulk solution experiments. Such metastable states can persist over long timescales before transforming into the thermodynamically stable state and might also be prevalent in ambient aerosol particles. In the following, we highlight some substances, whose polymorphism has been investigated using single particle techniques.

Glutaric acid exists in two crystalline forms that are enantiotropic to each other: the β-form is stable at room temperature, the α-form above 63 °C. The two forms can be well discriminated by Raman spectroscopy with the most apparent distinction in the C–H stretching region at 2800–3000 cm^{-1}. Yeung *et al.*[198] investigated glutaric acid single particles in EDB and flow cell experiments at ambient temperature and observed that rapid drying led to the crystallization of glutaric acid in the metastable α-form, which either deliquesced at 85–86% in a short time, or underwent polymorphic transformation to the β-form, which remained as a solid phase until 87–89%RH when slow water uptake started. In a similar single particle EDB study, Ehre *et al.*[199] found that glutaric acid crystals, which were formed at $>$ 40% by rapidly reducing the total pressure in the chamber below ~27–54 kPa, deliquesced at 85 ± 2% RH, consistent with the metastable α-form. Glutaric acid crystals formed at $\leq$ 30% RH at 101 kPa within 10 min after injection, deliquesced at 90 ± 2% RH, corresponding to the stable β polymorph. These observations might explain the variations in DRH ranging from 83 to 90% found in hygroscopic studies of glutaric acid (Table 1 of Yeung *et al.*[198]).

Ammonium nitrate (AN) exists in five polymorphic forms, designated as phases V, IV, III, II and I, which are all enantiotropic to each other. In atmospheric research, very little attention has been paid to the solid-solid phase transitions of AN because phase IV particles are stable over a wide range of tropospheric temperatures (*i.e.* −17°−32 °C). Wu *et al.*[200] have shown in an *in situ* microscopic FTIR spectroscopy study that single particles produced by efflorescence exhibit only the IV ↔ II transition at about 52 °C (forward) and 48 °C (reverse), bypassing phase III, which is stable between 32–52 °C. They conclude that the water content in AN, including the surface adsorption as a function of RH, significantly affects the IV → III phase transition, because this proceeds *via* dissolution and crystallization catalyzed by water. With *in situ* microscopic Raman spectroscopy, Wu and Chan[201] showed that addition of traces of other salts may change the phase transition behaviour of solid AN (40–700 μm) particles: with the addition of potassium nitrate, the IV → II transition, which appears at 52 °C for pure AN particles, is replaced by the IV → III transition. These results suggest that atmospheric solid AN particles may exist in phases IV and III. In mixtures with AS, AN can form double salts. Ling and Chan[202] found that equimolar AN/AS mixed droplets investigated in an EDB and analysed by Raman spectroscopy crystallized as a metastable 3AN·AS double-salt, which gradually transformed to the stable 2AN·AS double-salt. The rate of this transformation increased with increasing RH.

Due to the high solute supersaturations that can be reached in single particles, substances that form hydrates at ambient conditions often crystallize in an anhydrous form or turn into a glass because at ERH the solution is too concentrated to realize the stoichiometry of the hydrate that is stable in the presence of water. Tang and Fung[203] found such behaviour for $Ca(NO_3)_2$ particles in EDB experiments: from solution thermodynamics it is expected that anhydrous $Ca(NO_3)_2$ particles would transform into the tetrahydrate at 11.4%RH, which would then deliquesce at 50%RH. However, anhydrous particles deliquesced at 18%RH and the tetrahydrate has never been observed.

Upon evaporation, the solution droplets lost water and turned into amorphous particles, which contained one water molecule per solute and maintained their spherical shape. These examples show that single particle studies are indeed needed to derive solid state properties of aerosols consisting of substances that exhibit polymorphism.

III.f Future directions

It must be stressed that the phase behaviour, water partitioning and morphology of mixed component aerosol play a critical role in governing aerosol properties and this will become increasingly apparent in the discussion of aerosol properties and processes that follows. Thus, an improved understanding of aerosol microphysical properties is central to improving our understanding of aerosol in the atmosphere, as suggested by the centrality of these properties in Fig. 1. The examples in section *III.d* show that the investigation of particle morphology with single particle techniques is a challenging topic. The investigation of selected systems with different techniques should allow the development and validation of procedures for the interpretation and evaluation of experiments that then can be 'routinely' applied to determine morphologies of 'new' systems. One challenge is that all single particle techniques, with the exception of STXM, need supermicron particles for investigation. In principle, size should not influence the basic morphology given by surface and interfacial forces, but it might act on the complexity of the morphology: *e.g.* given a fully engulfed configuration based on the balance of interfacial and surface forces, the number of inclusions present in a particle will decrease with size. Such a particle size dependence of the number of minor phase inclusions was indeed observed by Ciobanu *et al.* for PEG-400/AS particles in the size range from 10–70 μm diameter.[43]

IV. Vapour pressures and gas-particle partitioning

In order to predict secondary organic aerosol concentrations in the atmosphere, an equilibrium partitioning framework such as that of Pankow is typically used.[204] Three key parameters needed for applying absorptive partitioning are the vapour pressures of the pure components as liquids (subcooled, if necessary), the enthalpy of vaporization of the subcooled liquid component and the activities of the components in the condensed phase. While it is certainly impossible to measure these parameters for all components occurring in the atmosphere, if only because of their sheer number,[11] single particle techniques may contribute decisively to the determination of vapour pressure, enthalpies of vaporization and activities of key model systems. The data of those model systems then can be used to parameterize activities for thermodynamic models such as E-AIM[205] and AIOMFAC[155] or vapour pressures for vapour pressure estimation models such as the method of Nannoolal *et al.*[206] or the EVAPORATION model.[207] However, the vapour pressure data available today, even for relatively simple systems such as the saturated straight-chain dicarboxylic acids, differ by up to two orders of magnitude between different measurement techniques![55,208] This difference seems to be even larger for some of the substituted dicarboxylic acids,[209] without an obvious explanation for these discrepancies being available at the moment.

Early on it was realized that measuring single particle evaporation rates may provide accurate vapour pressure data if certain conditions are fulfilled.[210] Single particle techniques offer the truly unique opportunity not only to perform measurements of the same substance in different physical states, but identify the state unambiguously. Since the precision in measuring very small size changes is very high (section II.b), single particle measurements are especially well suited to determine very low vapour pressures of semivolatile compounds at ambient temperatures, which are currently at the focus for better estimating atmospheric gas-particle partitioning. We will discuss the conditions and the theoretical basis for the measurements in the next section followed by a review of some measurements and a discussion of the associated uncertainties. A final section is devoted to the influence of physical state on vapour pressure.

IV.a Theoretical basis

The basis for understanding the quasi-stationary evaporation of single droplets was established by Maxwell in 1877[211] in a discussion of the wet bulb thermometer. Let us consider a spherical droplet motionless relative to a uniform gaseous medium with the particle radius, r, large compared to the mean free path λ_i of the evaporating species i, *i.e.* a Knudsen number $K_n = \lambda_i/r$ that is less than unity. In this limit, referred to as the continuum regime, the rate of evaporation is governed by gas phase diffusion if the vapour concentration at the droplet surface is assumed to be in equilibrium with the liquid phase:[212]

$$\frac{\mathrm{d}r^2}{\mathrm{d}t} = \frac{2D_{ij}M_i}{R_\rho}\left(\frac{p_\infty}{T_\infty} - \frac{p}{T}\right), \qquad (2)$$

where r is the radius of the particle, D_{ij} the gas diffusivity of i in the surrounding medium j, M_i is the molecular weight, ρ the density of the droplet, R the gas constant, p and p_∞ are the partial pressures of the species at the surface of the droplet and at infinite distance, respectively, and T and T_∞ the corresponding temperatures. The effect of curvature, that is the Kelvin effect, is neglected here, because the particles in typical single particle experiments are sufficiently large that the correction for curvature is negligible. We also limit our discussion to slow evaporation for which the droplet temperature can be assumed to be approximately the same as the ambient temperature, T_∞, and the partial pressure will converge to the vapour pressure of the species of interest.

If the Knudsen number is considerably larger than unity, *i.e.* the mean free path of the gas phase molecules is much larger than the particle radius, we can apply kinetic gas theory, sometimes referred to as the free-molecule regime. This yields a linear dependence of radius on time:[213]

$$\frac{\mathrm{d}r}{\mathrm{d}t} = -\frac{\alpha c_i p M_i}{4\rho RT}, \qquad (3)$$

c_i is the average speed of the species i: $c_i = (8RT/\pi M_i)^{1/2}$ and α is the evaporation (accommodation) coefficient. Roughly for $Kn \leq 0.05$, continuum diffusion theory applies, while for $Kn > 10$ kinetic theory applies.[213]

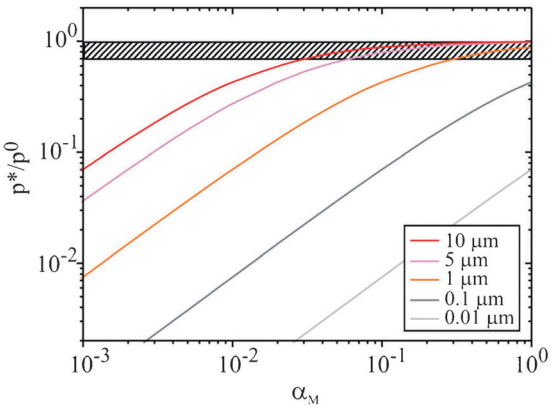

Fig. 10 An example of treating evaporation as solely governed by gas phase diffusion, *i.e.* neglecting mean free path and accommodation coefficient on vapour pressure estimates from evaporation rates. Ratio of estimated vapour pressure from evaporation rate measurements, p^*, to correct vapour pressure, p^0, *versus* accommodation coefficient for different radii of a glutaric acid particle evaporating at 283 K in air with a total pressure of 80 kPa.[215] The hatched area marks an underestimation in pressure with respect to the correct one of 0.7.

In the intermediate transition or Knudsen regime, with *Kn* being of the order of one, the Boltzmann rate equation needs to be solved to predict the mass transfer process. In this transition regime, different approximate corrections to eqn (2) have been suggested.[214] Here we discuss briefly the correction factor for the gas phase diffusivity D_{ij} given by Pruppacher and Klett for evaporation in the Knudsen regime.[215] In particular, it is instructive to calculate the effect of the accommodation coefficient on derived vapour pressure for conditions in this intermediate range of Knudsen numbers, as shown in Fig. 10. The vapour pressure estimate p^* is always smaller than the correct vapour pressure value p^0 when it is assumed that gas phase diffusion solely controls evaporation and surface kinetics (governed by the evaporation coefficient) are ignored. For particles with a radius larger than 1 μm, Fig. 10 shows the underestimation to be smaller than 30% if the evaporation coefficient is larger than about 0.3. Thus, for droplets with sizes typical of single particle experiments, we can conclude that Maxwell's eqn (2) may be safely applied for deducing vapour pressures. This makes evaporation experiments with single micron sized particles especially attractive, since no complex modelling or knowledge of surface tensions or evaporation/accommodation coefficients is required. Also it is technically easy to maintain a zero vapour pressure, p_∞, of the evaporating species far from the particle, which further simplifies the analysis of eqn (2).

Thus, measurements of size (or mass) *versus* time of a single, levitated particle allow the estimation of a number of important parameters for modelling gas to particle partitioning. If evaporation experiments are repeated with particles composed of the same substance in different gases over a wide range of pressures, not only can the vapour pressure of the substance be obtained, but gas phase diffusivities[216] of the evaporating molecules and the evaporation/mass accommodation coefficient[54,217] can be estimated. Since the diffusivities are functions of the Lennard-Jones interaction potential parameter and the collision diameter for unlike molecules, the parameters for the evaporating species can be obtained if the like-molecular parameters of the carrier gas are known.

If measurements are made of the size of an evaporating droplet consisting of a binary mixture into a gas phase in which one of the components (typically the component with the higher vapour pressure and often water) has a finite, constant concentration, the activity coefficients of the two components in solution can be obtained.[55,218,219] For example, to study the evaporation of a SVOC from an aqueous droplet, the water partial pressure (RH) must be maintained at a constant value. Then, the change in size with time reflects the evaporation of the organic component and the associated loss of water, such that the composition of the droplet does not change with time. Hence, the partial pressure of the SVOC in the binary mixture as measured from the mass flux is determined by its concentration within the mixture, its activity coefficient and its vapour pressure as a pure component. Repeating such evaporation experiments with different concentrations of the volatile component (*e.g.* experiments at different RHs) in the gas phase can allow determination of the concentration dependence of the activity. Activity coefficients can be obtained by even more complex measurements of size changes of binary or ternary droplets under unsteady state evaporation.[217,220]

IV.b Measurements and uncertainties

While early evaporation measurements on single levitated particles using a classical Millikan oil drop chamber were not satisfactorily reproducible,[212] Davis and Chorbajian[53] were the first to overcome the experimental difficulties using a modified Millikan cell enabling them to measure evaporation rates of dioctyl phthalate (DOP) in the continuum regime by tracking evolving size from phase function measurements. Later Davis and Ray[216] used the same principle to measure the rates of dibutyl sebacate droplets evaporating into helium, nitrogen, and carbon dioxide, see Fig. 11. Clearly, the data show the expected linear dependence of r^2 on time for continuum mass transport.

Richardson *et al.* were the first to perform evaporation experiments on single particles in the kinetic regime by levitating a sulphuric acid droplet in an EDB at 10^{-5} torr ambient pressure and estimating the change in particle size from the elastic scattering resonance spectrum.[112] The change in radius with time (Fig. 12) was linear when evaporating in vacuum, consistent with evaporation in the free-molecule regime, eqn (3). Ray *et al.*[26] also used an EDB for evaporation experiments in the kinetic regime, but increased the pressure of the medium to investigate transition regime evaporation.

Zardini *et al.*[115] used light scattering from a broad wavelength LED source (section II.b) to measure evaporation rates of aqueous dicarboxylic acid particles over a wide range of fixed relative humidities and at different temperatures yielding vapour pressures and activities (Fig. 13) of the dicarboxylic acids. To obtain activities a Clausius–Clapeyron relationship is assumed between vapour pressure, p^L, and temperature, T:

$$p^L(T) = p^{0,L}(T^\circ)a^{(x)} \exp\left[-\frac{\Delta H^\circ_{vap}}{R}\left(\frac{1}{T}-\frac{1}{T^\circ}\right)\right], \qquad (4)$$

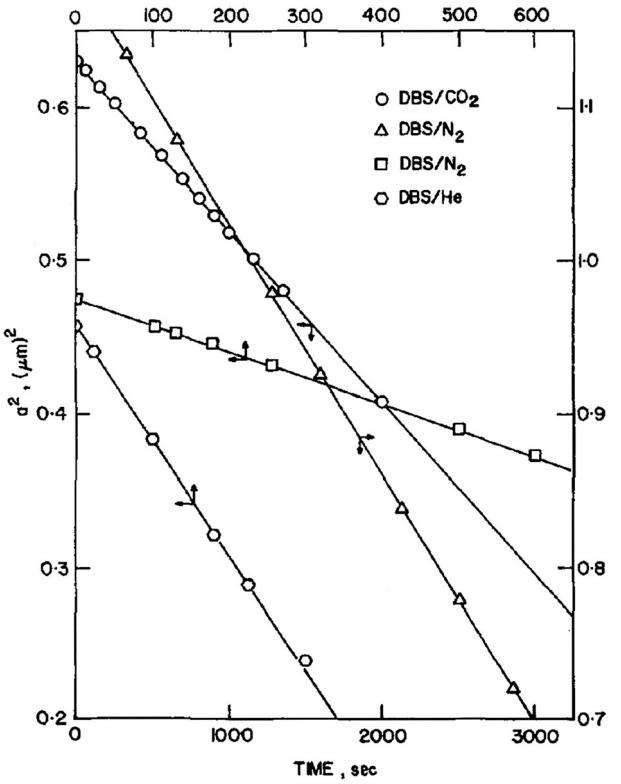

Fig. 11 Evaporation rates of DBS measured in different carrier gases to determine gas phase diffusivities, Lennard-Jones potential constants and vapour pressures simultaneously. All data show the linear dependence of radius squared with time as expected from Maxwell's equation. The slope in He is much steeper compared to the one in N_2 (circles and squares, left and upper axis), indicative of the larger diffusion constant of DBS in He relative to DBS in N_2. [Reprinted with permission from ref. 216, Copyright American Institute of Physics.]

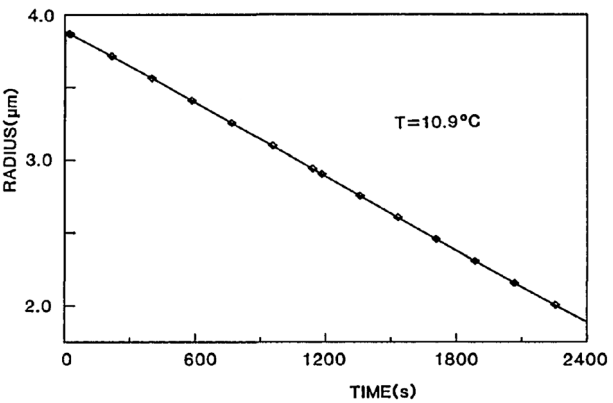

Fig. 12 A sulphuric acid droplet evaporating in a vacuum, showing a constant rate of change in radius as expected in the kinetic regime. [Reprinted with permission from ref. 112, Copyright Optical Society of America.]

with $p^{0,L}(T^\circ)$ being the subcooled liquid vapour pressure of the pure solute at $T^\circ = 298.15$ K, ΔH°_{vap} is the standard enthalpy change of vaporization, and $a^{(x)}$ is the mole fraction based activity.

While most of the earlier work used levitation of charged single particles in an electric field, more recently levitation by radiation pressure or trapping using optical tweezers have also been used to optically isolate single particles for evaporation rate measurements. Trunk *et al.*[221] used Raman spectroscopy to measure the relative concentration of the two components of a binary droplet evaporating. In addition they also used elastic Mie resonance spectroscopy for retrieval of size and refractive index simultaneously with the Raman measurements. They found good agreement between concentrations deduced from Raman spectroscopy and those obtained by retrieving refractive index from Mie resonance spectroscopy. Very recently an optical tweezers setup has been used to determine vapour pressures[222] from evaporating droplets in the continuum regime.

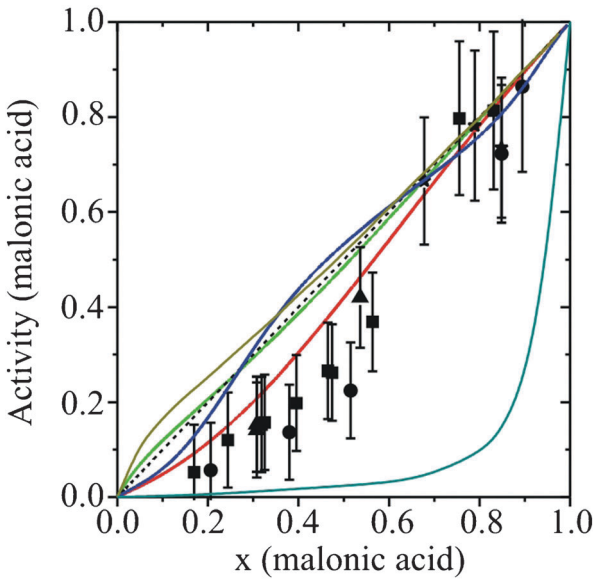

Fig. 13 Malonic acid activity, showing that data such as shown in Fig. 3 can be used to deduce activities. Symbols are data at different temperatures, lines are different thermodynamic models or parameterizations. The specific details of the models and parameterizations are not relevant here and the reader is referred to the original discussion for more information. [Reprinted with permission from ref. 55, Soonsin *et al.*]

In order to consider the errors associated with vapour pressure measurements made on single particles, we first assume that the evaporation rate itself, *i.e.* either the mass loss with time or the size change with time, can be measured without any error, focussing on the inherent uncertainties in some of the essential thermophysical parameters that appear in eqn (2) and (3). For measurements on particles of a single component in the continuum regime, the uncertainty in the gas phase diffusivity of the evaporating component determines the uncertainty associated with the vapour pressure. For most components there are no independent measurements of gas phase diffusivity and one relies typically on estimation methods for the Lennard Jones interaction potential parameters. The uncertainties of the estimated diffusivities are typically of the order of 20%, yielding a lower limit for the vapour pressure uncertainty. Clearly, if the diffusivity is explicitly accounted for by performing careful measurements in different carrier gases then this uncertainty can be reduced.[216] If size is measured and not mass, the density of the condensed phase has to be estimated or measured, although its uncertainty is typically considerably smaller than

the one for the diffusivity. In the kinetic regime it is the uncertainty in the evaporation coefficient which dominates the total uncertainty in vapour pressure. It is standard practice to assume an evaporation coefficient of unity because there are no independent measurements available for most systems of atmospheric interest. However, again an uncertainty of 20% is easily conceivable.

Experimentally, a significant source of error can be the uncertainty in the partial pressure of the evaporating component far from the particle, usually assumed to be negligible, $p_\infty = 0$. For very low volatile material, even some spurious particles deposited on the walls of a cell may lead to a failing of this assumption. This leads to underestimation of the vapour pressure, which may also vary from experiment to experiment. For binary, aqueous particles, which are of special interest to the atmospheric community, an additional error arises from the precision of the relative humidity (or water vapour pressure) measurement. A ± 2% error is often unavoidable when capacitance probes are used for relative humidity determination, which leads to a significant error in concentration estimate. The measurement uncertainty of the change in particle size over time can usually be assumed to be much smaller than the uncertainties already discussed, particularly when the particles are liquid and one can take advantage of the extremely high precision of Mie scattering sizing.

IV.c Vapour pressures and the physical state

As stated in the introduction, single particle techniques offer the unique opportunity to detect the physical state of the particle unambiguously, see also section II. Whether a particle is of spherical symmetry or not can be easily distinguished based on the two–dimensional angular optical scattering pattern,[223] intensity fluctuations of the scattered light,[124] or the presence of WGMs.[191] Thus, vapour pressure measurements are possible for particles in both the liquid and solid states with the same instrument. If the particle under investigation is water soluble, three distinct vapour pressures may be measured: the vapour pressure of the subcooled liquid, the vapour pressure of the aqueous, saturated solution, and the vapour pressure of the solid. From fundamental thermodynamics considerations we know the vapour pressure of the saturated solution and that of the solid to be the same. The vapour pressure of the subcooled liquid can be calculated from that of the solid if the enthalpy of fusion and the change in heat capacity between the liquid and solid state at the triple point are known.[224]

An example for the strength of the method is shown in an application to dicarboxylic acids in Fig. 14. First, the vapour pressures of the solids agree with those of the corresponding saturated solutions for the measurements of Soonsin *et al.*[55] as required by thermodynamics. Second, these measurements strongly support the interpretation that Bilde *et al.*[225] measured the vapour pressure of the supersaturated solution in case of malonic (C3) and glutaric acid (C5) and of the solid in case of the succinic acid (C4) in TDMA measurements. Cappa *et al.*[226] measured the vapour pressures of succinic and glutaric acid in their solid state in agreement within error with those of

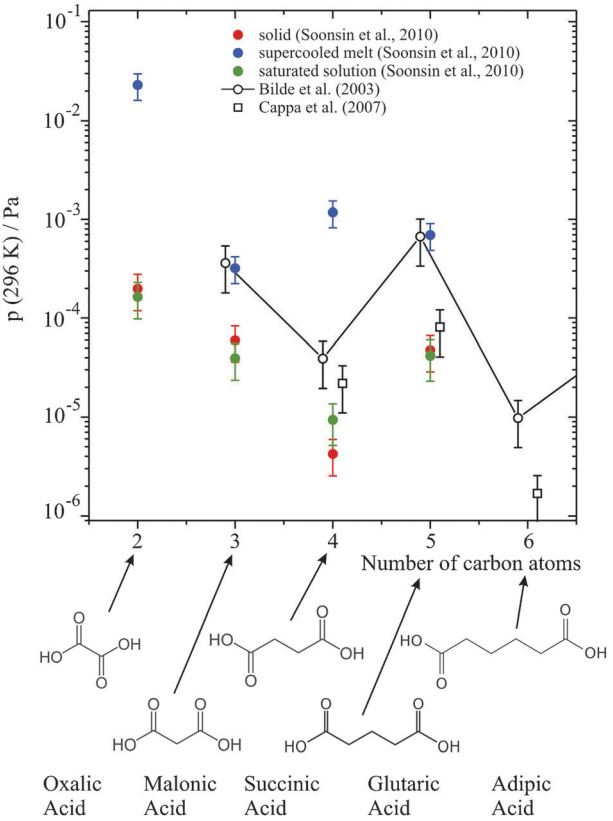

Fig. 14 Vapour pressures of straight chain dicarboxylic acids *versus* carbon number of the acids. Selected data from the literature are compared to data from single particle measurements with identification of physical state. [Reprinted with permission from ref. 55, Soonsin *et al.*]

the vapour pressures of the saturated solutions of Soonsin *et al.*[55] Without considering the physical state of the particles, discrepancies in vapour pressure of about an order of magnitude might be assigned to the different techniques, while in fact the measurements agree most likely within error if the phase is correctly identified.

Another interesting observation of the single particle study[55] was that a freshly effloresced succinic acid particle exhibits the evaporation rate of the supersaturated solution, slowly decreasing with time and with an evaporation rate in r^2 consistent with the solid vapour pressure only after 1 day. This was interpreted as an indication that the solid did not crystallize in the thermodynamically stable form, but that the effloresced particle contained significant solvent inclusions and/or defective crystal structures. Evaporation of the solvent must first occur, before the evaporation rate can be reconciled to that expected for the thermodynamically stable, defect free solid.

IV.d Future directions

Further investigations are needed to see how much of the large differences in vapour pressure obtained with different techniques can be explained by the inherent uncertainties when deriving vapour pressures of the subcooled liquid state from measurements performed in the solid state. To avoid potential problems, we recommend that the vapour pressures in the subcooled liquid state be measured whenever possible.

However, even evaporation measurements in the subcooled liquid state with the same setup often show scatter not easily explained by careful error analysis.[209,222] A step forward to more reliable data could be achieved by performing evaporation experiments with the same setup in both the kinetic and continuum regime, preferably even with the same particle.

V. Mass transport of water limited by surface or bulk phase kinetics

Quantifying the rate of condensation or evaporation of water from aerosol particles is crucial for understanding the partitioning of water between the gas and condensed phases in the atmosphere. Although it is often assumed that the partitioning of water is governed by thermodynamics, there are instances where this may not be the case, notably during the activation and growth of CCN and IN, and in the transport of water to and from amorphous or glassy aerosol.[227,228] In the former case, it is important to quantify the transport of water through the surface region, referred to as surface kinetics.[51] The condensing or evaporating flux is dependent on the probability that a water molecule reaching the surface either adsorbs or evaporates, respectively. For adsorption, this probability has been referred to as the mass accommodation coefficient, although more recently this has been more correctly designated as the surface accommodation coefficient.[51,52] For evaporation, the probability is referred to as the evaporation coefficient and is assumed equal to the surface accommodation coefficient by microscopic reversibility.[229] In the activation of CCN in warm clouds, it has been shown that the cloud droplet number concentration is sensitive to the exact value of the accommodation coefficient.[230] If the value is close to unity, the more hygroscopic particles activate and grow rapidly, constraining the maximum level of the supersaturation reached in a rising air parcel and suppressing the activation of less hygroscopic aerosol. If the value is less than 0.1, the slower growth of the more active CCN allows the supersaturation to rise to a higher value and more CCN are activated leading to higher cloud droplet number.

The suggestion by Zobrist *et al.*[46] that atmospheric aerosol can form glasses has been confirmed by Virtanen *et al.*[47] for secondary organic aerosol at low RH. The persistence of aerosol in glassy states or highly viscous solutions, rather than crystalline solids, could have profound consequences for understanding the transport of water, SVOCs and reactive species in the bulk of aerosol particles. Kinetic inhibition of crystallization and water transport could affect the potential of SOA to act as IN or CCN, affecting the cloud droplet number concentration.[46] Shiraiwa *et al.* have investigated the influence of particle bulk viscosity on atmospheric aging, estimating that oxidation of organic compounds embedded within atmospheric particles at moderate RH can take place on a time scale of hours.[231] Rather than the transport of water and other species being governed by surface kinetics, diffusion within the particle bulk is extremely slow and the kinetics of evaporation or condensation can be limited by diffusional gradients within the particle bulk or even the transport of molecules from the surface into the near-surface bulk, now often quantified by the bulk accommodation coefficient.[45,46,51]

Single particle measurements have provided important insights into the factors governing both surface and bulk accommodation, complementing studies on aerosol ensembles. Indeed, in the case of bulk accommodation, single particle studies have led the way. We shall consider these two processes in turn, principally focussing on the transport of water between the gas and condensed phases.

V.a Surface accommodation

The earliest studies to examine the influence of surface kinetics on water transport from single droplets were performed by Davis and co-workers on droplets trapped within an EDB using elastic light scattering to measure droplet radius.[102,107] Droplets were injected into dry nitrogen gas and the decrease in droplet size during evaporation measured with a time resolution of $\sim$0.2 s. Taflin *et al.* reported measurements of the evaporation of pure water droplets over $\sim$2 s and the first measurement of the influence of a surfactant, sodium dodecyl sulphate (SDS), on the evaporation of water.[107] Droplet sizes started from 20 to 30 μm radius and diminished to $<$ 5 μm. For the evaporation of water droplets of such size at atmospheric pressure, the transport of water is limited by gas phase diffusion in the continuum regime and is insensitive to surface kinetics (as shown in Fig. 10). Droplet evaporation is initially unsteady, but a wet bulk temperature lower than the ambient temperature is rapidly achieved, limiting the evaporative flux that can be sustained by heat transport from the gas phase to the droplet surface.[62]

In the case of the evaporation of water droplets containing SDS, the observations of Taflin *et al.* showed that the rate of evaporation was observed to suddenly decline by more than 2 orders of magnitude after $\sim$1 s of water evaporation, suggesting that the formation of an organic film on the surface of the droplet was impeding water transport and decreasing the mass flux.[107] Similar results were later recorded by Shulman *et al.* for the evaporation of aqueous solution droplets of oxalic acid, adipic acid, *cis*-pinonic acid, SDS and ammonium sulphate, the latter two examples shown in Fig. 15.[102] For these measurements, it was suggested that the formation of an insoluble coating was responsible for the slowing of the evaporation rate. A correlation between the surface tension and the solution concentration at which the evaporation rate slowed was found and it was suggested that organic films could significantly alter the rate of water transport, going beyond what would be simply expected based on vapour pressure depression due to the solute effect. Given the very similar behaviour seen for this wide range of binary droplets including the non-surface-active AS salt, we instead consider that it is likely that the droplets have reached an equilibrium state and then the subsequent drift in size may be due to slow RH drifts in the measurement. Recent work by Davies *et al.*[70] has shown that the estimation of the dry size can be significantly in error if the initial droplet size recorded is assumed to have the same concentration as the initial bulk solution.

Zientara *et al.* (2008) reported values of the evaporation coefficient of water, measured from water droplets, 5–10 μm in radius, evaporating in an EDB at RHs above 90%.[232] Although the exact water saturation value was not measured,

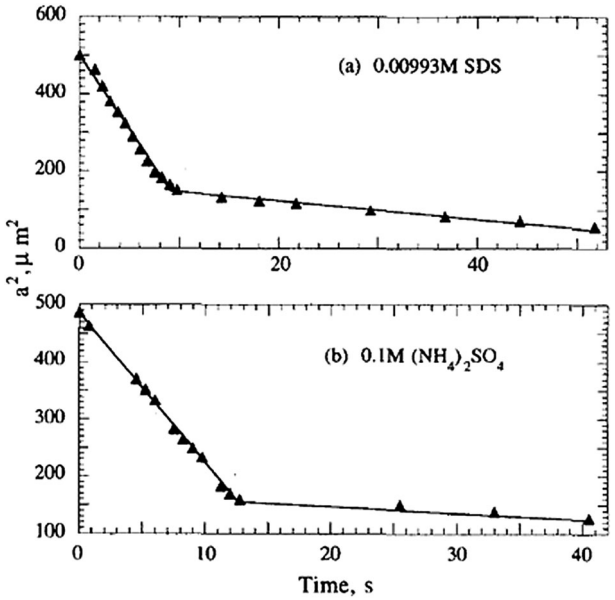

Fig. 15 Time dependencies of the radius squared for evaporating aqueous solution droplets with the initial concentrations of sodium dodecyl sulphate and ammonium sulphate indicated. Evaporation was into humidified nitrogen at a temperature of 282 K and at a RH of 77 and 84% for (a) and (b), respectively. [Reprinted with permission from ref. 102, Copyright Elsevier.]

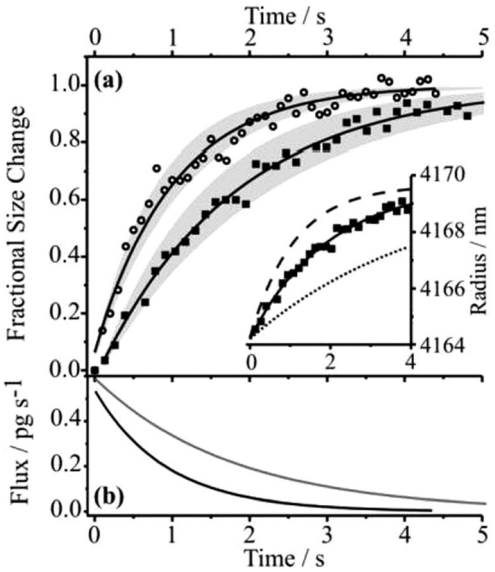

Fig. 16 (a) Comparison of the envelopes of measured equilibration events (grey shaded) observed at 6.5 kPa (circles and fit line, one event) and 100 kPa (squares and fit line, one event) during the condensation of water on a tweezed aqueous sodium chloride droplet. The inset shows the absolute radius during a single event compared with the model predictions (dashed line, neglecting latent heat; dotted line, latent heat dissipated into the gas phase at steady droplet temperature). (b) Mass fluxes estimated from the kinetic fits for the low (black line) and high (grey line) pressure events in (a). [Reprinted with permission from ref. 240, Copyright American Physical Society.]

they were able to simulate their measurements to retrieve the RH from the early time data, allowing the evaporation coefficient to be estimated from the longer time behaviour of the droplet evaporation. In addition, they measured the temperature dependence of the evaporation coefficient over the range 273 to 293 K, finding a trend that was consistent with droplet train measurements and a mass accommodation coefficient that increased from ~0.12 at the highest temperature to ~0.32 at the lowest temperature.[232–234] These values should be compared with values measured from a liquid jet evaporating in vacuum[235–237] and expansion chamber measurements, both of which reported values that were consistently higher, in the range 0.6 to 1.0.[238,239] Clearly, further work is needed to better constrain the values of the accommodation and evaporation coefficients.

Miles *et al.* have recently reported the development of a new strategy for investigating condensation and evaporation kinetics using optical tweezers.[240] A solution droplet is held within an optical trap and its size estimated with sub-nanometre accuracy from the WGMs apparent in the Raman fingerprint. The gradient force trap is sufficiently strong that droplets can be retained within the trap even to low pressure, typically a lower limit of ~2 kPa that is set by the vapour pressure of water. Although light absorption of the laser beam at 532 nm used to trap the droplet is very weak in the visible part of the electromagnetic spectrum, a low level of optical heating is induced equivalent to a temperature elevation above the ambient gas phase of ~10 mK.[240] Introducing or removing a second laser beam leads to the introduction or removal of a small additional perturbation equivalent to a few mK. On introducing the heating beam, the droplet warms marginally and water must evaporate from the droplet, increasing the solute concentration, and returning the droplet to equilibrium with the gas phase. Conversely removal of the heating beam leads to a marginal cooling and condensation of water occurs. In both cases, the droplet size changes by typically ~2 nm. An example is shown in Fig. 16. This approach provides an opportunity to examine the kinetics of condensation and evaporation on the same droplet in quick succession and to resolve the two processes with approaching molecular layer resolution. Measurements of the kinetics of size change as a function of pressure reveal the importance of understanding the transfer of latent heat to or from the droplet, particularly at low pressure. Although not yet allowing a definitive value of surface accommodation coefficient to be determined, such an approach can provide considerable detail in investigating mass transfer at the surface of aerosol particles.

V.b Bulk accommodation

Zobrist *et al.* were the first to examine the influence of glass formation on the water transport to and from a single aerosol particle.[49] Using sucrose as a proxy for oxidised organic components in the atmosphere, with a convenient glass transition RH at ambient temperature (~25% RH), they examined the change in particle size with change in RH for sucrose particles 5–8 μm in radius held in an EDB. At ambient temperature, particles showed contrasting behaviour at RHs below and above 40% during repeated drying and humidifying cycles, as seen in Fig. 17. At high RHs, it was found that a particle responded rapidly to changes in RH and could be assumed to exist in equilibrium with the surrounding vapour phase.

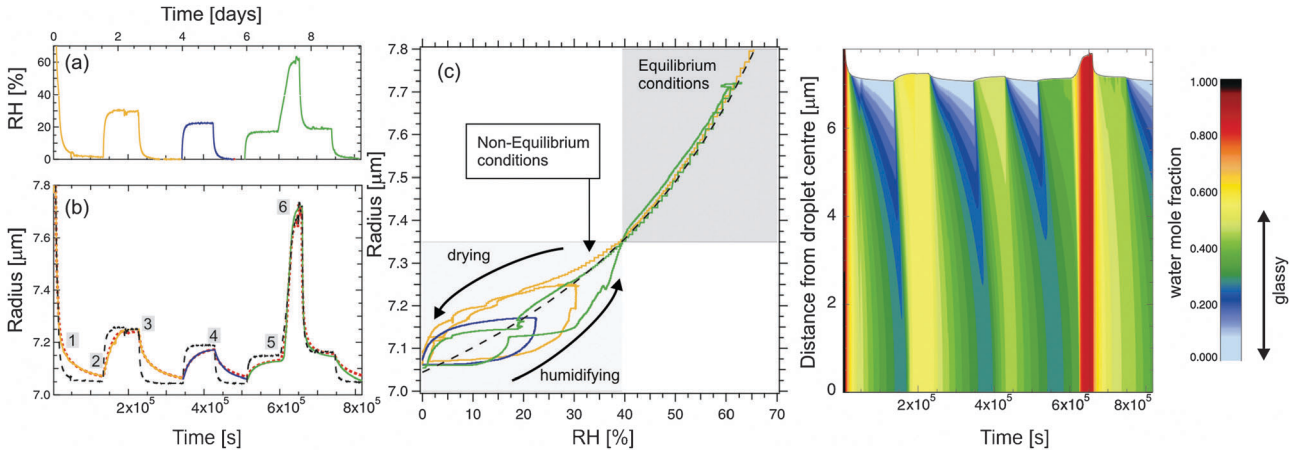

Fig. 17 Humidity cycles for a single aqueous sucrose particle investigated at 291 K. Panels (a) and (b) show, respectively, the chamber relative humidity (RH) and the particle's radius as a function of time (coloured solid lines). Panel (c) shows the particle's radius as a function of RH (same data as in (a) and (b)). The dashed black line in (b) and (c) indicate conditions of thermodynamic equilibrium between the particle and gas phase humidity. The red dotted line in (b) shows calculated radius using a numerical spherical shell model for condensed phase diffusion. Panel (d) shows the particle's radial concentration profile as a function of time calculated with the liquid-phase diffusion model. [Reprinted with permission from ref. 49, Copyright Royal Society of Chemistry.]

At low RHs, considerable delay in the size change accompanying a change in RH was observed. Indeed, on attempting to dry a particle at 0% RH, the particle radius was found to continuously shrink over a time frame of 10^5 s, never reaching a steady equilibrium size.

Water transport within the particle bulk was recognised by Zobrist *et al.* as being a highly non-linear diffusion process, requiring numerical solution of the spherical diffusion equation.[49] A spherical shell diffusion model was developed, allowing the inhomogeneity in particle composition, and thus the water diffusion coefficient, to be treated explicitly. Rather than the creeping diffusion tails usually expected, the numerical solutions were shown to lead to steep diffusion fronts or waves, often referred to as Marshak-waves, as is evident from the simulations of the radial concentration gradients of water shown in Fig. 17. The model was shown to successfully reproduce the time-dependent trends in particle size accompanying both changes in RH at 291 K and with variation in temperature down to 200 K. Considerable variation in water mole fraction within the particle was predicted with water diffusion coefficients expected to decrease from 10^{-9} m^2 s^{-1} in the solution phase at ambient temperature to as low as 10^{-24} m^2 s^{-1} in the glassy phase at 200 K, the lowest value that could be experimentally measured. Such a large variation in diffusion constant can be expected to have profound consequences for water transport in aerosol in the upper troposphere and lower stratosphere in particular, and more generally for the transport of SVOCs and reactive species in atmospheric aerosol.

Reinforcing many of the conclusions of the single particle work of Zobrist *et al.* using an EDB, Tong *et al.* used optical tweezers to investigate the hygroscopicity of sucrose aerosol from dry conditions to $>$ 70% RH at room temperature.[48] The spherical shell diffusion model reported by Zobrist *et al.*[49] was used to simulate the time-dependence of particle size in the tweezers for droplets from 3 to 4 μm in radius and excellent agreement was found for RH changes of 5–10% starting at 43% to as low as 6%, as shown in Fig. 18. At the lowest RH,

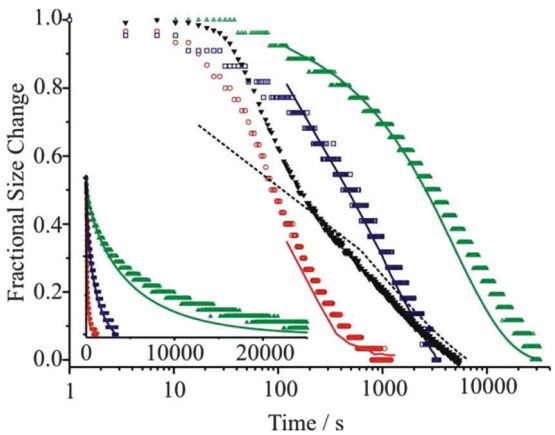

Fig. 18 The measured response in the size of sucrose droplets following four changes in RH (red, 43 to 36.7%; blue, 26 to 16.3%; green, 6.6 to 0%; black, 45.6 to 1.6%). The experimental data are shown by the symbols and the results of kinetics simulations using the ETH model are shown by the solid lines. The inset shows three of the size changes on a linear timescale. [Reprinted with permission from ref. 48, Tong *et al.*]

it was possible to allow the particle to sediment to the coverslip, a few 10's micrometres below the optical trap by turning off the laser beam. Unlike the spreading and loss of particle shape observed for solution droplets, the particles were observed to retain their spherical shape, even to the extent of continuing to support WGMs. This is consistent with studies of the bounce factor of ambient secondary organic aerosol at low RH on impactor stages made by Virtanen *et al.* who concluded that the particles had mechanical properties similar to those expected of solid particles.[47]

Similar behaviour in delayed water transport was observed for raffinose particles and also for ternary mixtures of sucrose, sodium chloride and water. Indeed, the latter work suggested that even for viscous liquid droplets, the kinetics of water transport were slowed considerably at RH $<$50%.[48] Bones *et al.* expanded the range of kinetic studies of bulk accommodation of water

for the ternary solution droplets of sucrose/sodium chloride/water.[241] Not only did these measurements provide further evidence for the slowing of water transport in highly viscous solution droplets, but they suggested that the time-response in particle size can be correlated to the bulk viscosity of the particle at a particular water activity providing a method for estimating timescales for water transport based on the Stokes–Einstein equation.

Li *et al.* have also investigated the kinetic limitations imposed on water transport by the formation of a gel phase in aqueous magnesium sulphate droplets, monitoring the exchange of D_2O by H_2O in droplets initially formed just by deuterated aqueous solutions.[42] Unlike glassy states, a gel consists of a phase separated system and, in the case of magnesium sulphate, contact ion pairs between the ionic components form at low RH and are thought to form polymeric chain. A porous network results through which water can diffuse only slowly; the elongated path that water must take to leave the particle leads to an apparent slowing in water transport. At RHs below 40%, the timescale for replacement of residual D_2O by H_2O was shown to require many hours in particles 20–60 μm in diameter.

V.c Future directions

Although sucrose has been used as a benchmark system for exploring the influence of a glassy state on water transport, it is important that further measurements explore the mechanism of water transport in a broader range of organic components relevant to SOA and in complex mixtures with inorganic components. Based on the correlation observed by Bones *et al.* between the timescale for size change and the bulk viscosity, an extrapolation of the observed behaviour for the coarse mode particles studied in EDB and tweezers experiments was reported to particle sizes in the accumulation mode.[241] However, it is crucial that the validity of these extrapolations be assessed, particularly the extrapolation to particle sizes in the accumulation mode. From the time dependence of the WGMs apparent in the Raman fingerprint of sucrose particles, Bones *et al.* were able to confirm the presence of steep diffusional fronts during the condensation of water on the surface of a glassy particle and the progressive dissolution of the core.[241] Such measurements should allow a refinement of the microphysical spherical diffusion model used to simulate water transport in glassy aerosol.

VI. Oxidation kinetics and mechanisms

There are particular challenges associated with studying heterogeneous aerosol chemistry in the laboratory. Smog chamber studies have yielded many important insights, but are demanding and large in scale, requiring the deployment of numerous analytical techniques.[242,243] Measurements are often performed at dry conditions and the dependence on RH has been only infrequently investigated. Measurements are performed on particles covering a size distribution and it is not possible to directly resolve the interplay of gas and condensed phase chemistry and gas/particle partitioning in governing particle size and composition without complex simulations; particles must be extracted from the chamber ending the processing of the particular sample under study. However, oxidant concentrations, particle concentrations and size distributions can be kept at values relevant to the atmosphere, and photochemistry and gas phase chemistry can be regulated appropriately. Aerosol flow tube studies, while allowing a better constraint to be placed on parameters such as the particle size distribution, are limited in timescale and studies must often be performed at elevated gas phase oxidant concentrations, although the dependence on RH can be explored.[244,245]

Single particle studies can be pursued at oxidant concentrations directly relevant to the atmosphere. Direct signatures of the time dependence of the reactant loss, product formation and reaction kinetics can be achieved from *in situ* non-intrusive techniques such as Raman spectroscopy or from the evolving mass or diameter of a particle. The timescale for the volatilisation of products can be separated from reaction chemistry. The morphology/phase of the particle can often be directly observed by brightfield imaging. The RH can be controlled, allowing hygroscopic growth measurements to be made and the influence of RH on the chemistry to be explored. In addition, all of these measurements can be made on a single particle. A limitation of this approach is that measurements have only been made on coarse mode particles so far, from a few microns in size to many 10's of microns, and the significance of these studies for accumulation mode particles must be inferred. We highlight below studies that have examined: the product branching during the ozonolysis of organic aerosol; the reaction kinetics and volatilisation of semi-volatile products; the RH dependence of the reaction mechanism; and the hygroscopicity of the oxidised aerosol.

VI.a Identifying products

Lee and Chan reported the first study of oxidative aging of organic aerosol using an EDB[56] examining the oxidative processing of oleic acid aerosol by ozone under dry (<5% RH) conditions and at ozone concentrations as low as 240 ppb. Oleic acid was investigated as distinct Raman signatures of the carbon-carbon double bond (Stokes shift of 1655 cm^{-1}) can be used to monitor the disappearance of the reactant. Between 50–80% of the oleic acid reacted over a timescale of 20 h for two particles of different initial size. The appearance of Raman signatures from oxygenated functional groups was considered to be consistent with the expected mechanism of ozonolysis and results reported from other techniques.[246,247] Observed Raman signatures include: the appearance of O–O stretching vibrations from peroxides and/or ozonides; C=O stretching vibrations from aldehydes, ketones, carboxylic acids and esters: and O–H stretching vibrations from compounds that may include alcohols, carboxylic acids and hydroperoxides. The Raman signatures from droplets oxidised at much higher ozone concentration (>10 ppm) were also recorded and found to be consistent with the measurements made at much lower ozone concentration.

Lee and Chan also studied the oxidation of the conjugated variants of oleic acid, linoleic acid and linolenic acid with two and three carbon-carbon double bonds, respectively.[57] At the same low ozone concentration considered for oleic acid, the evolving Raman signatures were shown to be consistent with the evolution in products from autoxidation processes,

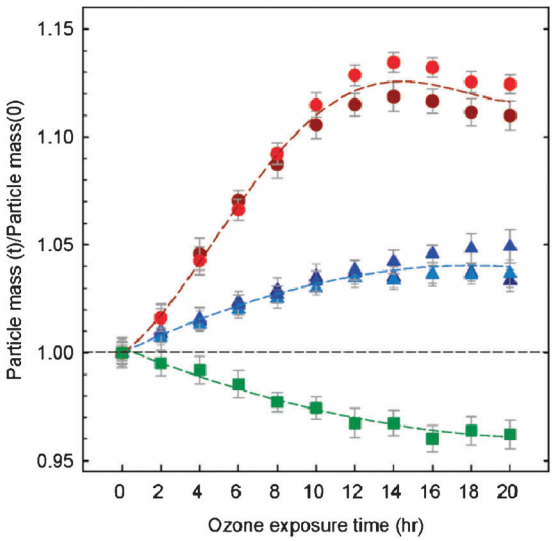

Fig. 19 Changes in mass for oleic acid (green squares, one particle), linoleic acid (blue triangles, three particles) and linolenic acid (red circles, two particles) particles during ozone exposure periods. The lines are to guide the eye and have no physical meaning. The ozone concentration in each experiment was 200–250 ppb. [Reprinted with permission from ref. 57, Copyright 2007 American Chemical Society.]

typical free radical chemistry involving chain initiation, propagation and termination steps. The possibility of autoxidation processes cannot occur for oleic acid at typical ambient temperatures. By comparison, at high ozone concentrations (~10 ppm), it was concluded that the Raman signatures were consistent with the dominance of typical ozonolysis chemistry. Contrary to the observations for oleic acid aerosol, the autoxidation mechanism was found to lead to an increase in the mass of linoleic acid and linolenic acid particles during the first 10 h of the experiment due to the formation of products of low volatility, as shown in Fig. 19.

King *et al.* reported the first application of an optical trapping technique (optical tweezers) for studying a heterogeneous gas-particle reaction, investigating the ozonolysis of solutions of oleic acid and synthetic seawater on droplets 5–9 μm in diameter at RHs greater than 95%.[248] The ozone concentration and oleic acid volume fraction were not reported. However, clear Raman signatures for the production of nonanoic acid and nonanal were observed during oxidation with nonanal disappearing promptly and nonanoic acid taking hundreds of seconds to disappear, presumably a consequence of their different volatilities.

It should be stressed here that the systems studied so far by Raman spectroscopy have been chosen for their relative chemical simplicity. The reactants have been shown to have distinctive spectroscopic fingerprints and the products are few and well established. With increasing chemical complexity, the overlap of distinctive Raman signatures becomes increasingly problematic and the determination of evolving composition becomes ambiguous. In addition, if molecules with aromatic functionality are present, a strong fluorescence background may obscure the Raman scattering signal.

VI.b Volatilisation of products and product branching ratios

During the ozonolysis of oleic acid, a particle can be expected to gain mass from the addition of oxygenated functionalities in the oxidised products, but can also be expected to lose mass by the volatilisation of volatile and semi-volatile products. Indeed, although Lee and Chan observed a loss of between 50 and 80% of the oleic acid reactant over the course of 20 h, the particle mass was observed to decline by only between 1 and 4%, Fig. 19.[56] The product branching between volatile components (nonanal and nonanoic acid), semi-volatile products (and azelaic acid) and involatile oligomeric products was not resolved.

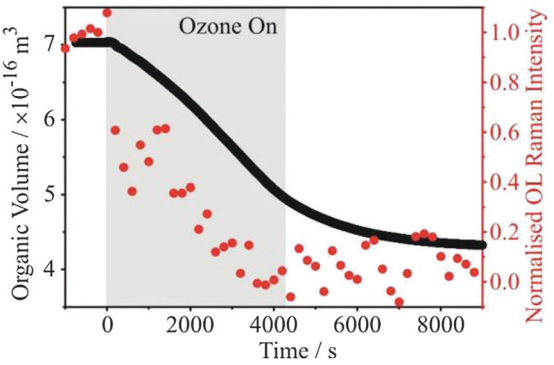

Fig. 20 Temporal evolution of the organic volume (black line) as measured from the CERS fingerprint and the normalised oleic acid Raman signal intensity (vinylic CH stretch) during ozonolysis of an oleic acid droplet containing an effloresced NaCl seed. The ozone flow was turned on during the period shown by the grey box with a concentration of ~3 ppm. The oxidation was carried out under dry (<5% RH) conditions. [Reprinted with permission from ref. 61, Copyright 2012 American Chemical Society.]

Recently, Dennis-Smither *et al.* have used optical tweezers to study the oxidation of oleic acid droplets containing an inorganic seed under dry conditions and at an ozone concentration of ~3 ppm, with time-resolution sufficient to resolve the reactive loss of ozone and the evaporative loss of products.[61] As well as observing the characteristic disappearance of the Raman signatures from oleic acid, the resonant enhancement in the Raman signal at WGMs wavelengths was used to quantify the change in droplet size over time, Fig. 20. Although the oleic acid reacted to completion in ~3000 s, the droplet volume continued to evolve over a further 5000 s due to the slow volatilisation of reaction products. Nonanoic acid (vapour pressure ~0.2 Pa at 25 °C) and 9-oxononanoic acid (estimated as ~0.02 Pa) were judged to have vapour pressures that would lead to their evaporation on timescales of 100 and 1000 s, respectively, consistent with the measured rate of evaporative loss. Nonanal (~40 Pa), with a much higher vapour pressure, was expected to evaporate on the timescale of its production. An involatile organic core remained over timescales of many hours, with a volume equivalent to 60 ± 5% of the initial organic phase volume, presumably composed of azelaic acid and involatile oligomeric products and consistent with previous aerosol flow tube studies.[249,250]

VI.c Ozonolysis kinetics

Currently, to our knowledge there is only one report that attempted a quantitative kinetic analysis of reactive aerosol processing recorded from measurements on single aerosol particles. King *et al.*[251] investigated the oxidation kinetics of biogenic and water-soluble compounds in aqueous and organic

aerosol droplets by ozone, specifically examining the ozonolysis of fumarate anions and benzoate anions in aqueous solution and α-pinene in dodecane or pentadecane, the latter serving as a proxy for organic atmospheric aerosol.[251] Typical ozone concentrations were between 0.4 and 1.0 ppm and the disappearance of the reactants was monitored by Raman scattering. In all cases, the rate of evaporation of the organic component was at least a factor of four slower than the rate of loss by reaction. The aqueous solution aerosol reactions were carried out at a constant RH of 60 to 80%. No systematic change in the size of the aerosol was observed during the course of the reaction within an uncertainty of ± 0.25 μm. While the aqueous phase reactions occurred over a time frame of >3000 s, the reaction of α-pinene occurred on a timescale of hundreds of seconds. The kinetic analysis of the data demonstrated that the reactant loss rate was limited by liquid phase diffusion and reaction rate in particle bulk, with ozone diffusion in the gas phase and mass accommodation at the droplet surface rapid by comparison.

VI.d The relative humidity variable: changes in hygroscopic growth and reaction mechanism

A tendency for the products of heterogeneous chemistry to be more highly oxygenated than the reactants suggests that they should also be more water soluble and display a greater degree of hygroscopic growth with increase in RH. Although King *et al.*[251] observed the clear disappearance of the reactant fumarate and benzoate anions when the RH was held constant at 60–80%, there was no apparent increase in droplet size due to hygroscopic growth within the uncertainty of their measurements, ± 0.25 μm. This was considered to be consistent with the initial low starting mole fractions of the reactants which were stated as > 0.0015. The reaction of α-pinene occurred in a hydrocarbon matrix with the appearance of oxygenated functionality in the Raman spectra. No increase in size that could be attributed to hygroscopic growth was observed, even at 60% RH.

Dennis-Smither *et al.* recorded the hygroscopic growth of oleic acid droplets prior to and post oxidation under dry conditions.[61] The highly sensitive Raman measurements allowed the determination of growth factors between 1.002 and 1.004 at 72% RH prior to oxidation and 1.006 and 1.015 after oxidation, corresponding to growths in size of only ~16 nm and ~60 nm for a 4 μm droplet radius before and after oxidation, respectively. These diameter growth factors were found to be consistent with estimates from the mass growth factors reported from EDB measurements by Lee and Chan of 1.0007 ± 0.0017 and 1.004 ± 0.002 for particles before and after partial oxidation of oleic acid.[25,56,57] These growth factors were also found to be consistent with measurements made on accumulation mode particles in a flow reactor.[250] Surprisingly, King *et al.* reported an increase in particle size of up to 1.5 μm for a 6.5 μm diameter aqueous solution droplet containing predominantly inorganic salts.[248] The reasons for such a large change in size remain unclear.

Not only is it important to consider the changes in hygroscopicity that accompany oxidative aging, but the influence of water vapour on reaction mechanism must be considered. Pope *et al.* explored the oxidation of maleic acid by ozone in an EDB.[252] On exposure of a solid maleic acid particle to ozone under dry conditions, no apparent change in particle mass was observed. However, increasing the RH above the deliquescence point was found to initiate chemistry, even though the ozone flow had been terminated. On drying the particle once again, the evaporation of volatile components into the gas phase was observed, clearly demonstrating that water plays an important role in determining the mechanism for the reaction of maleic acid. This is an excellent example of the advantages of performing measurements on single particles: properties such as component vapour pressures and hygroscopicities can be measured for the same particle at various points during an oxidation cycle, providing unique information on transformation pathways.

VI.e Future directions

This is an appropriate point at which to consider the unique way in which single particle measurements can help improve our understanding of heterogeneous chemistry. As highlighted by the final example above, the presence of water in a particle can clearly change the reaction mechanism suggesting that it may be crucially important to investigate the influence of elevated RH on reaction mechanisms in the condensed phase, and to contrast behaviour with effloresced and deliquesced inorganic seed particles. Even if the mechanism is not altered, it is possible that the reaction kinetics may be very different, either due to the dependence of bulk phase diffusion constants of reactive species on water partitioning to the condensed phase or due to the changes in the surface-to-volume ratio of the organic phase that accompany the phase separation of hydrophobic and hydrophilic domains. Recently, Chan and Chan have investigated the role of the phase state and water content in governing the ozonolysis of internal mixtures of maleic acid and ammonium sulphate particles with the aqueous phase reaction occurring more rapidly than reaction with a crystalline solid particle.[253] Measurements such as those shown in Fig. 20 should provide an accurate method for mapping out reaction kinetics and their dependence on environmental conditions. In addition, given the likely prevalence of oligomer formation for many systems, the kinetics of hygroscopic growth for unprocessed and processed particles must be compared.

Miles *et al.* have recently shown that the complex refractive index of optically trapped aerosol droplets can be determined with high accuracy, ± 0.11% for the real part and as good as ± 0.5 × 10^{-9} for the complex part.[122] Using such an approach to examine the time dependence of the refractive index of a droplet during heterogeneous processing could be invaluable in proving compositional changes, inferring density changes, and examining browning reactions. Recently it has been shown that photomediated chemistry may have a strong effect on aerosol oxidative aging.[254,255] For example the uptake coefficient of ozone on bulk HULIS solution increased by one order of magnitude under irradiation (300–420 nm, 1.7 × 10^{15} photons cm^{-2} s^{-1}). Single particle experiments are well suited to quantify photochemical aging and its dependence on environmental conditions in future studies.

Returning to the centrality of identifying the microphysical state of aerosol for understanding the processing of aerosols (Fig. 1),

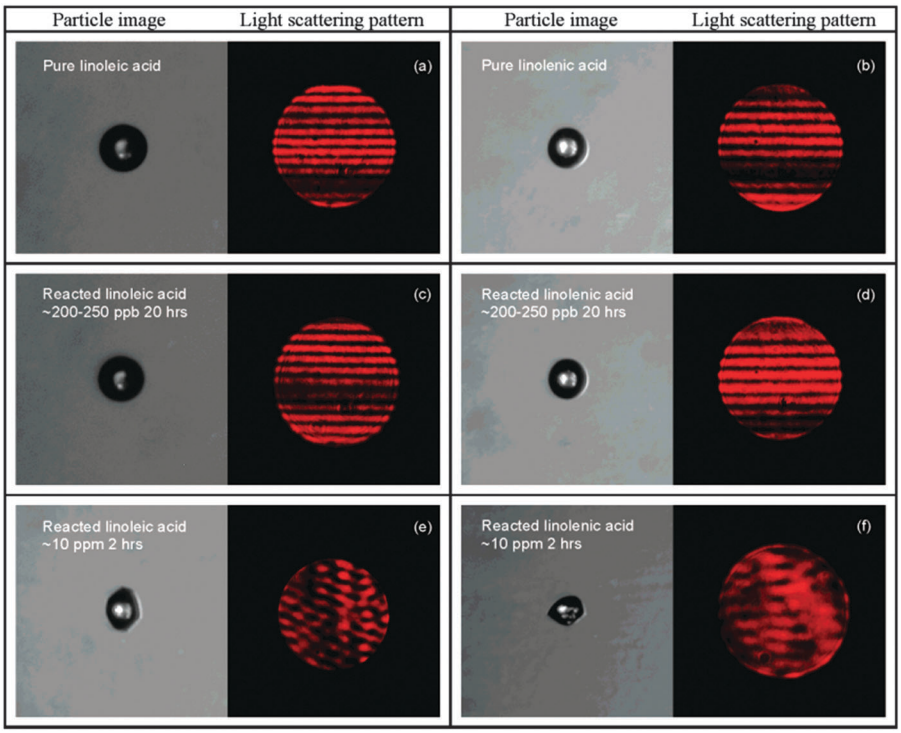

Fig. 21 Particle images and laser-illuminated light scattering patterns of the pure and ozone-processed linoleic acid (left-hand side) and linolenic acid particles (right-hand side). [Reprinted with permission from ref. 57, Copyright 2007 American Chemical Society.]

Lee and Chan showed that the final state of the processed aerosol can even be dependent on the oxidant concentrations.[25,57] The reactive processing of linoleic and linolenic acids by ozone showed that processing at higher concentration (10 ppm compared with 200–250 ppb) resulted in particles that departed from spherical and were irregular, Fig. 21. Indeed, it has been suggested that the resulting oxidised aerosol may show resistance to water uptake leading to delayed growth and a kinetic inhibited water transport.

Not only must the thermodynamic and kinetics factors governing the partitioning of water between the condensed and gas phases be considered, but the partitioning of other semi-volatiles, such as ammonia and amines, must be more fully explored, along with the dependence of the partitioning on environmental conditions. Chan and Chan have recently reported the displacement of ammonia by triethylamine from particles initial composed of a range of ammonium salts.[256] The same authors have also studied the dependence of nonanal partitioning between acidic aerosol particles and gas phases and the enhancement that can result when organic components are present.[257] Many of these examples highlight the role of reactive uptake in governing the partitioning of semi-volatile components to the condensed aerosol phase.

Quantifying the influence of the processing conditions on the final properties of the particle requires attention, and can be directly investigated using single particle techniques. Currently, much of the information on changes in chemical speciation that occur during heterogeneous chemistry is acquired from Raman measurements. While this technique is invaluable for studying systems of relative simplicity containing only a few components, studying complex chemical mixtures that more closely resemble atmospheric aerosol may require new tools for *in situ* direct analysis. Principal component analysis can allow the identification of characteristic Raman fingerprints from complex overlapping bands, even when fluorescing chromophores are present, and this approach has yet to be applied to studies of heterogeneous aging in single particle measurements. There are techniques used in bulk analysis to reject the fluorescent background in Raman scattering such as deep UV resonance Raman spectroscopy, shifted excitation Raman difference spectroscopy, or pulsed excitation with gated detection, *e.g.* Sinfield *et al.*[258] The application of these techniques to single particle Raman spectroscopy has yet to be explored. Alternatively, as with many other aerosol techniques, characterisation may be limited to post-analysis (*e.g.* by combining with single-particle mass spectrometry) or by indirect measurements of composition (*e.g.* the retrieval of particle refractive index).

VII. Concluding remarks

In this review, we have presented a wide spectrum of laboratory studies that have aimed at improving the understanding of microphysical properties and transformation processes occurring at the single particle level. Only when these detailed findings are considered in models of atmospheric aerosol can they help to lessen the uncertainties connected with aerosol forcings. This link between laboratory studies and model development is mostly directed at predicting the thermodynamic properties of aerosols. Vapour pressure and activity data from single particle studies are an important source for parameterizing vapour pressure estimation models like EVAPORATION and thermodynamic models like E-AIM and AIOMFAC. The collaboration between modellers and

experimentalists should be cultivated so that single particle studies indeed investigate systems that are needed to fill the most urgent gaps in thermodynamic models. Here, experimentalists have to face the additional challenge that most of the still remaining gaps involve reactive substances like aldehydes, peroxides and olefins, which require an even tighter control of composition to discriminate between reactive and thermodynamic properties.

It must be noted that the single particle techniques reviewed here are applicable only to particles in the coarse mode, >2 μm in diameter. It is important to recognise that such large particles represent only a very small fraction of the number concentration of particles in the atmosphere, with most particles in the accumulation mode, <1 μm in diameter. Given this, the relevance of single particle measurements is often questioned. For some properties, such as phase behaviour, hygroscopic growth and component vapour pressures, measurements made on coarse particles can lead to simplification of the measurement, decoupling the bulk and surface curvature effects that determine the property. Measurements made on coarse mode particles provide values that are independent of surface curvature, providing invaluable insight to measurements made on accumulation mode particles that are a convolution of bulk and surface effects. Surface curvature effects are well understood and can be easily accounted for when extrapolating measurements on coarse particles to smaller particles sizes. Of course such extrapolation requires additional data on surface properties, *e.g.* surface tension. Conclusions drawn on particle morphology, particularly liquid–liquid phase separations, will be equally valid for particles of all but the smallest size (<100 nm). Perhaps the two areas where the relevance of single particle measurements must be most closely examined are the kinetics of gas-particle partitioning and of heterogeneous chemistry. However, in both of these cases, the detailed information that can be achieved with these approaches is unprecedented, far surpassing that from measurements made on accumulation mode particles. Indeed, the measurements of evolving composition, refractive index, inhomogenieties in composition, and size that can be made over lengthscales from the nanometre to the micrometre and over timescales spanning from the millisecond to the hour can provide robust and invaluable data for the validation of complex kinetic models. If these models can be validated on particles ranging in size from 2 to 100 μm, a factor of 10^5 change in volume, the application of the same models to smaller particles should not be considered to incur significant error. Of course, single particle measurements on accumulation mode particles would be invaluable in validating such models to smaller sizes and new approaches do exist that are extending single particle measurements to such sizes.[94,95,259]

The need to understand the link between microphysical properties, chemical composition and the timescale for aerosol transformation and processing has been highlighted most recently in the recognition that an aerosol rich in organic components may exist in a glassy or amorphous state.[47,227] Persistence in such a state can inhibit the transport of water, semi-volatile organics and reactive species between the gas and condensed phases. Failing to identify aerosol as existing in a glassy or amorphous state has important consequences for understanding the water content and optical properties of the aerosol, and could prolong the lifetimes of organic components in the aerosol phase. Just as importantly, understanding the influence of the microphysical state on the temporal response of the aerosol during hygroscopic growth may even be critical to interpreting the data acquired from common analytical techniques such as hygroscopic measurements made by tandem differential mobility analysers. The examples given in this review show that single particle studies have a great potential to resolve chemical and physical processes and to relate them to the physical state of the particles.

To improve gas/particle partitioning schemes in regional and global models, prediction of chemical reaction pathways, identification of the time limiting processes and the particles microphysical state need to go hand in hand because the partitioning of a semi-volatile organic component (SVOC) between the condensed and gas phases may depend on liquid–liquid phase separations and the morphology of hydrophobic and hydrophilic phases in the particles. Further, the evolution of quantities such as the single scattering albedo are dependent on time-dependent heterogeneity in particle composition and the validity of using mixing rules for predicting the optical properties of aerosol that may be complex in phase and morphology.

The reduction of such complex behaviour to simple parameterizations for regional and global models is an endeavour that needs close interaction of modellers and experimentalists and will keep them busy in the upcoming years. The large gap that still exists between the detailed knowledge obtained from single particle studies and the crude assumptions implemented in large scale models should therefore not frustrate the experimentalist and prevent them from going forward.

Acknowledgements

JPR wishes to acknowledge the EPSRC for funding and support of a Leadership Fellowship.

References

1 G. McFiggans, *et al.*, *Atmos. Chem. Phys.*, 2006, **6**, 2593–2649.
2 M. Hallquist, *et al.*, *Atmos. Chem. Phys.*, 2009, **9**(14), 5155–5236.
3 J. L. Jimenez, *et al.*, *Science*, 2009, **326**(5959), 1525–1529.
4 Q. Zhang, *et al.*, *Geophys. Res. Lett.*, 2007, **34**(13).
5 D. M. Murphy, *et al.*, *J. Geophys. Res.*, 2006, **111**(D23), D23s32.
6 C. Marcolli and U. K. Krieger, *J. Phys. Chem. A*, 2006, **110**(5), 1881–1893.
7 C. Marcolli, B. P. Luo and T. Peter, *J. Phys. Chem. A*, 2004, **108**(12), 2216–2224.
8 E. Weingartner, M. Gysel and U. Baltensperger, *Environ. Sci. Technol.*, 2002, **36**(1), 55–62.
9 U. Baltensperger, *et al.*, *Faraday Discuss.*, 2005, **130**, 265–278.
10 M. N. Chan, M. Y. Choi, N. L. Ng and C. K. Chan, *Environ. Sci. Technol.*, 2005, **39**(6), 1555–1562.
11 A. H. Goldstein and I. E. Galbally, *Environ. Sci. Technol.*, 2007, **41**(5), 1514–1521.
12 S. Fuzzi, *et al.*, *Atmos. Chem. Phys.*, 2006, **6**, 2017–2038.
13 G. McFiggans, D. O. Topping and M. H. Barley, *Atmos. Chem. Phys.*, 2010, **10**(21), 10255–10272.
14 M. O. Andreae and A. Gelencser, *Atmos. Chem. Phys.*, 2006, **6**, 3131–3148.
15 M. Posfai and P. R. Buseck, *Annu. Rev. Earth Planet. Sci.*, 2010, **38**, 17–43.
16 R. C. Moffet, *et al.*, *Atmos. Chem. Phys.*, 2010, **10**(3), 961–976.

17 A. Zuend, C. Marcolli, T. Peter and J. H. Seinfeld, *Atmos. Chem. Phys.*, 2010, **10**(16), 7795–7820.
18 M. A. Freedman, K. J. Baustian, M. E. Wise and M. A. Tolbert, *Anal. Chem.*, 2010, **82**(19), 7965–7972.
19 Y. Liu, *et al.*, *Phys. Chem. Chem. Phys.*, 2011, **13**(25), 11846–11857.
20 M. E. Wise, K. J. Baustian and M. A. Tolbert, *Proc. Natl. Acad. Sci. U. S. A.*, 2010, **107**(15), 6693–6698.
21 A. K. Bertram, *et al.*, *Atmos. Chem. Phys.*, 2011, **11**(21), 10995–11006.
22 C. A. Colberg, U. K. Krieger and T. Peter, *J. Phys. Chem. A*, 2004, **108**(14), 2700–2709.
23 C. Marcolli, *et al.*, *Geochim. Cosmochim. Acta*, 2009, **73**(13), A832–A832.
24 J. P. Reid, *et al.*, *Phys. Chem. Chem. Phys.*, 2011, **13**(34), 15559–15572.
25 A. K. Y. Lee, T. Y. Ling and C. K. Chan, *Faraday Discuss.*, 2008, **137**, 245–263.
26 A. K. Ray, J. Lee and H. L. Tilley, *Langmuir*, 1988, **4**(3), 631–637.
27 J. P. Reid, *J. Quant. Spectrosc. Radiat. Transfer*, 2009, **110**(14–16), 1293–1306.
28 J. P. Reid, H. Meresman, L. Mitchem and R. Symes, *Int. Rev. Phys. Chem.*, 2007, **26**(1), 139–192.
29 A. Ashkin, *Phys. Rev. Lett.*, 1970, **24**, 156.
30 A. Ashkin and J. M. Dziedzic, *Appl. Phys. Lett.*, 1971, **19**(8), 283.
31 L. Mitchem and J. P. Reid, *Chem. Soc. Rev.*, 2008, **37**, 756–769.
32 J. B. Wills, K. J. Knox and J. P. Reid, *Chem. Phys. Lett.*, 2009, **481**(4–6), 153–165.
33 E. J. Davis, *Aerosol Sci. Technol.*, 1997, **26**(3), 212–254.
34 E. J. Davis, M. F. Buehler and T. L. Ward, *Rev. Sci. Instrum.*, 1990, **61**(4), 1281–1288.
35 E. J. Davis, P. Ravindran and A. K. Ray, *Adv. Colloid Interface Sci.*, 1981, **15**(1), 1–24.
36 B. A. Al Zaitone and C. Tropea, *Chem. Eng. Sci.*, 2011, **66**(17), 3914–3921.
37 N. J. Mason, *et al.*, *Faraday Discuss.*, 2008, **137**, 367–376.
38 A. Kavouras and G. Krammer, *Rev. Sci. Instrum.*, 2003, **74**(10), 4468–4473.
39 A. Pant, M. T. Parsons and A. K. Bertram, *J. Phys. Chem. A*, 2006, **110**(28), 8701–8709.
40 B. J. Murray, S. L. Broadley, T. W. Wilson, J. D. Atkinson and R. H. Wills, *Atmos. Chem. Phys.*, 2011, **11**(9), 4191–4207.
41 M. Song, C. Marcolli, U. K. Krieger, A. Zuend and T. Peter, *Atmos. Chem. Phys.*, 2012, **12**(5), 2691–2712.
42 K.-K. Li, F. Wang, G. Zeng, J. P. Reid and Y.-H. Zhang, *J. Phys. Chem. B*, 2011, **115**(49), 14397–14403.
43 V. G. Ciobanu, C. Marcolli, U. K. Krieger, U. Weers and T. Peter, *J. Phys. Chem. A*, 2009, **113**(41), 10966–10978.
44 C. D. Cappa, E. R. Lovejoy and A. R. Ravishankara, *Proc. Natl. Acad. Sci. U. S. A.*, 2008, **105**(48), 18687–18691.
45 E. Mikhailov, S. Vlasenko, S. T. Martin, T. Koop and U. Poschl, *Atmos. Chem. Phys.*, 2009, **9**, 9491–9522.
46 B. Zobrist, C. Marcolli, D. A. Pedernera and T. Koop, *Atmos. Chem. Phys.*, 2008, **8**(17), 5221–5244.
47 A. Virtanen, *et al.*, *Nature*, 2010, **467**(7317), 824–827.
48 H. J. Tong, J. P. Reid, D. L. Bones, B. P. Luo and U. K. Krieger, *Atmos. Chem. Phys.*, 2011, **11**(10), 4739–4754.
49 B. Zobrist, *et al.*, *Phys. Chem. Chem. Phys.*, 2011, **13**(8), 3514–3526.
50 Y. Rudich, *Chem. Rev.*, 2003, **103**, 5097–5124.
51 C. E. Kolb, *et al.*, *Atmos. Chem. Phys.*, 2010, **10**(21), 10561–10605.
52 P. Davidovits, C. E. Kolb, L. R. Williams, J. T. Jayne and D. R. Worsnop, *Chem. Rev.*, 2006, **106**(4), 1323–1354.
53 E. J. Davis and E. Chorbajian, *Ind. Eng. Chem. Fundam.*, 1974, **13**(3), 272–277.
54 E. J. Davis and A. K. Ray, *J. Aerosol Sci.*, 1978, **9**(5), 411–422.
55 V. Soonsin, A. A. Zardini, C. Marcolli, A. Zuend and U. K. Krieger, *Atmos. Chem. Phys.*, 2010, **10**(23), 11753–11767.
56 A. K. Y. Lee and C. K. Chan, *Atmos. Environ.*, 2007, **41**(22), 4611–4621.
57 A. K. Y. Lee and C. K. Chan, *J. Phys. Chem. A*, 2007, **111**(28), 6285–6295.
58 J. D. Hearn, A. J. Lovett and G. D. Smith, *Phys. Chem. Chem. Phys.*, 2005, **7**(3), 501–511.
59 A. G. Carlton, *et al.*, *Atmos. Environ.*, 2007, **41**(35), 7588–7602.
60 B. Ervens, B. J. Turpin and R. J. Weber, *Atmos. Chem. Phys.*, 2011, **11**(21), 11069–11102.
61 B. J. Dennis-Smither, K. L. Hanford, N.-O. A. Kwamena, R. E. H. Miles and J. P. Reid, *J. Phys. Chem. A*, 2012, in press.
62 E. J. Davis and G. Schweiger, *The airborne microparticle: its physics, chemistry, optics, and transport phenomena*, Springer, Berlin, New York, 2002, p. 833p xiv, .
63 G. Schweiger, *J. Aerosol Sci.*, 1990, **21**(4), 483–509.
64 M. F. Hamilton and D. T. Blackstock, *Nonlinear acoustics*, Academic Press, 1998.
65 R. A. Millikan, *Phys. Rev.*, 1909, **30**, 560.
66 R. A. Millikan, *Science*, 1910, **32**, 436.
67 H. Straubel, *Z. Elektrochem.*, 1956, **60**(9–10), 1033–1036.
68 R. F. Wuerker, H. Shelton and R. V. Langmuir, *J. Appl. Phys.*, 1959, **30**, 342.
69 C. Heinisch, J. B. Wills, J. P. Reid, T. Tschudi and C. Tropea, *Phys. Chem. Chem. Phys.*, 2009, **11**(42), 9720–9728.
70 J. F. Davies, A. E. Haddrell and J. P. Reid, *Aerosol Sci. Technol.*, 2011, **46**(6), 666–677.
71 F. Weritz, A. Simon and T. Leisner, *Environ. Sci. Pollution Res.*, 2002, 92–99.
72 M. Y. Choi and C. K. Chan, *J. Phys. Chem. A*, 2005, **109**(6), 1042–1048.
73 A. Ashkin and J. M. Dziedzic, *Appl. Opt.*, 1981, **20**(10), 1803–1814.
74 R. Thurn and W. Kiefer, *J. Raman Spectrosc.*, 1984, **15**(6), 411–413.
75 T. R. Lettieri and R. E. Preston, *Opt. Commun.*, 1985, **54**(6), 349–352.
76 C. Esen, T. Kaiser and G. Schweiger, *Appl. Spectrosc.*, 1996, **50**(7), 823–828.
77 J. Musick, J. Popp, M. Trunk and W. Kiefer, *Appl. Spectrosc.*, 1998, **52**(5), 692–701.
78 M. Trunk, J. Popp, M. Lankers and W. Kiefer, *Chem. Phys. Lett.*, 1997, **264**(1–2), 233–237.
79 C. Mund and R. Zellner, *ChemPhysChem*, 2003, **4**(6), 630–638.
80 D. McGloin, *et al.*, *Faraday Discuss.*, 2008, **137**, 335–350.
81 A. Ashkin and J. M. Dziedzic, *Science*, 1975, **187**(4181), 1073–1075.
82 K. Schaschek, J. Popp and W. Kiefer, *J. Raman Spectrosc.*, 1993, **24**(2), 69–75.
83 C. Mund and R. Zellner, *J. Mol. Struct.*, 2003, **661–662**, 491–500.
84 J. E. Molloy and M. J. Padgett, *Contemp. Phys.*, 2002, **43**(4), 241–258.
85 A. Ashkin, J. M. Dziedzic, J. E. Bjorkholm and S. Chu, *Opt. Lett.*, 1986, **11**(5), 288–290.
86 M. D. Summers, D. R. Burnham and D. McGloin, *Opt. Express*, 2008, **16**(11), 7739–7747.
87 R. J. Hopkins, L. Mitchem, A. D. Ward and J. P. Reid, *Phys. Chem. Chem. Phys.*, 2004, **6**(21), 4924–4927.
88 J. P. Reid, *et al.*, Optical manipulation of aerosol particle arrays, in *Optical Trapping and Optical Micromanipulation VIII*, ed. K. S. G. C. Dholakia, 2011, vol. 8097.
89 J. Buajarern, L. Mitchem and J. P. Reid, *J. Phys. Chem. A*, 2007, **111**, 13038–13045.
90 A. M. C. Laurain and J. P. Reid, *J. Phys. Chem. A*, 2009, **113**(25), 7039–7047.
91 J. Buajarern, L. Mitchem and J. P. Reid, *J. Phys. Chem. A*, 2007, **111**(37), 9054–9061.
92 D. R. Burnham and D. McGloin, *Opt. Express*, 2006, **14**(9), 4175–4181.
93 J. R. Butler, *et al.*, *Lab Chip*, 2009, **9**(4), 521–528.
94 A. E. Carruthers, J. P. Reid and A. J. Orr-Ewing, *Opt. Express*, 2010, **18**(13), 14238–14244.
95 H. Meresman, J. B. Wills, M. Summers, D. McGloin and J. P. Reid, *Phys. Chem. Chem. Phys.*, 2009, **11**(47), 11333–11339.
96 M. D. Summers, J. P. Reid and D. McGloin, *Opt. Express*, 2006, **14**(14), 6373–6380.
97 T. Koop, H. P. Ng, L. T. Molina and M. J. Molina, *J. Phys. Chem. A*, 1998, **102**(45), 8924–8931.
98 H. Meresman, A. J. Hudson and J. P. Reid, *Analyst*, 2011, **136**(17), 3487–3495.
99 H.-J. Tong, J. P. Reid, J.-L. Dong and Y.-H. Zhang, *J. Phys. Chem. A*, 2010, **114**(46), 12237–12243.

100 J. P. Reid and L. Mitchem, *Annu. Rev. Phys. Chem.*, 2006, **57**, 245–271.
101 P. Ravindran and E. J. Davis, *J. Colloid Interface Sci.*, 1982, **85**(1), 278–288.
102 M. L. Shulman, R. J. Charlson and E. J. Davis, *J. Aerosol Sci.*, 1997, **28**(5), 737–752.
103 J. F. Widmann and E. J. Davis, *Aerosol Sci. Technol.*, 1997, **27**(2), 243–254.
104 D. Duft and T. Leisner, *Int. J. Mass Spectrom.*, 2004, **233**(1–3), 61–65.
105 A. K. Ray, A. Souyri, E. J. Davis and T. M. Allen, *Appl. Opt.*, 1991, **30**(27), 3974–3983.
106 I. N. Tang and H. R. Munkelwitz, *J. Geophys. Res.*, 1994, **99**(D9), 18801–18808.
107 D. C. Taflin, S. H. Zhang, T. Allen and E. J. Davis, *AIChE J.*, 1988, **34**(8), 1310–1320.
108 V. Devarakonda and A. K. Ray, *J. Colloid Interface Sci.*, 2000, **221**, 104.
109 D. C. Taflin and E. J. Davis, *J. Aerosol Sci.*, 1990, **21**(1), 73–86.
110 R. K. Chang and Y. L. Pan, *Faraday Discuss.*, 2008, **137**, 9–36.
111 R. Symes, R. M. Sayer and J. P. Reid, *Phys. Chem. Chem. Phys.*, 2004, **6**(3), 474–487.
112 C. B. Richardson, R. L. Hightower and A. L. Pigg, *Appl. Opt.*, 1986, **25**(7), 1226–1229.
113 A. K. Ray, V. Devarakonda and Z. Q. Gao, *Faraday Discuss.*, 2008, **137**, 85–98.
114 A. K. Ray, B. Devakottai, A. Souyri and J. L. Huckaby, *Langmuir*, 1991, **7**(3), 525–531.
115 A. A. Zardini, U. K. Krieger and C. Marcolli, *Opt. Express*, 2006, **14**(15), 6951–6962.
116 J. D. Eversole, *et al.*, *J. Opt. Soc. Am. B*, 1993, **10**(10), 1955–1968.
117 H. B. Lin and A. J. Campillo, *Opt. Lett.*, 1995, **20**(15), 1589–1591.
118 A. Biswas, H. Latifi, R. L. Armstrong and R. G. Pinnick, *Phys. Rev. A: At., Mol., Opt. Phys.*, 1989, **40**(12), 7413–7416.
119 J. Popp, *et al.*, *Appl. Spectrosc.*, 1998, **52**(2), 284–291.
120 J. Popp, *et al.*, *J. Raman Spectrosc.*, 1997, **28**(7), 531–536.
121 L. Mitchem, *et al.*, *J. Phys. Chem. A*, 2006, **110**(26), 8116–8125.
122 R. E. H. Miles, J. S. Walker, D. R. Burnham and J. P. Reid, *Phys. Chem. Chem. Phys.*, 2012, **14**(9), 3037–3047.
123 J. Buajarern, L. Mitchem and J. P. Reid, *J. Phys. Chem. A*, 2007, **111**, 11852–11859.
124 U. K. Krieger and C. Braun, *J. Quant. Spectrosc. Radiat. Transfer*, 2001, **70**(4–6), 545–554.
125 F. Zheng, M. L. Laucks and E. J. Davis, *J. Aerosol Sci.*, 2000, **31**(10), 1173–1185.
126 U. K. Krieger and A. A. Zardini, *Faraday Discuss.*, 2008, **137**, 377–388.
127 A. A. Zardini and U. K. Krieger, *Opt. Express*, 2009, **17**(6), 4659–4669.
128 A. A. Zardini and U. K. Krieger, *Opt. Express*, 2010, **18**(10), 10760–10761.
129 D. Baumgardner and A. Clarke, *J. Geophys. Res.*, 1998, **103**(D13), 16525–16534.
130 C. A. Colberg, B. P. Luo, H. Wernli, T. Koop and T. Peter, *Atmos. Chem. Phys.*, 2003, **3**, 909–924.
131 S. T. Martin, *et al.*, *Atmos. Chem. Phys.*, 2004, **4**, 183–214.
132 J. Wang, D. J. Jacob and S. T. Martin, *J. Geophys. Res.*, 2008, **113**(D11), D11207.
133 C. A. Randles, L. M. Russell and V. Ramaswamy, *Geophys. Res. Lett.*, 2004, **31**(16).
134 D. R. Collins, *et al.*, *Tellus, Ser. B*, 2000, **52**(2), 498–525.
135 X. H. Liu and J. A. Wang, *Environ. Res. Lett.*, 2010, **5**(4), 044010.
136 I. J. George and J. P. D. Abbatt, *Nat. Chem.*, 2010, **2**(9), 713–722.
137 N. F. Taylor, *et al.*, *Atmos. Chem. Phys.*, 2011, **11**(23), 12085–12107.
138 S. T. Martin, *Chem. Rev.*, 2000, **100**(9), 3403–3453.
139 M. N. Chan, A. K. Y. Lee and C. K. Chan, *Environ. Sci. Technol.*, 2006, **40**(22), 6983–6989.
140 M. T. Parsons, J. L. Riffell and A. K. Bertram, *J. Phys. Chem. A*, 2006, **110**(26), 8108–8115.
141 M. C. Yeung, A. K. Y. Lee and C. K. Chan, *Aerosol Sci. Technol.*, 2009, **43**(5), 387–399.
142 V. G. Ciobanu, C. Marcolli, U. K. Krieger, A. Zuend and T. Peter, *J. Phys. Chem. A*, 2010, **114**(35), 9486–9495.
143 M. Y. Choi and C. K. Chan, *Environ. Sci. Technol.*, 2002, **36**(11), 2422–2428.
144 T. Y. Ling and C. K. Chan, *J. Geophys. Res.*, 2008, **113**(D14), D14205.
145 M. T. Parsons, D. A. Knopf and A. K. Bertram, *J. Phys. Chem. A*, 2004, **108**(52), 11600–11608.
146 M. C. Yeung and C. K. Chan, *Aerosol Sci. Technol.*, 2010, **44**(4), 269–280.
147 L. Treuel, S. Pederzani and R. Zellner, *Phys. Chem. Chem. Phys.*, 2009, **11**(36), 7976–7984.
148 A. Pant, A. Fok, M. T. Parsons, J. Mak and A. K. Bertram, *Geophys. Res. Lett.*, 2004, **31**(12).
149 L. Treuel, S. Schulze, T. Leisner and R. Zellner, *Faraday Discuss.*, 2008, **137**, 265–278.
150 A. A. Zardini, *et al.*, *Atmos. Chem. Phys.*, 2008, **8**(18), 5589–5601.
151 S. Sjogren, *et al.*, *J. Aerosol Sci.*, 2007, **38**(2), 157–171.
152 M. N. Chan and C. K. Chan, *Environ. Sci. Technol.*, 2003, **37**(22), 5109–5115.
153 M. N. Chan and C. K. Chan, *Atmos. Environ.*, 2007, **41**(21), 4423–4433.
154 M. T. Parsons, J. Mak, S. R. Lipetz and A. K. Bertram, *J. Geophys. Res.*, 2004, **109**(D6), D06212.
155 A. Zuend, *et al.*, *Atmos. Chem. Phys.*, 2011, **11**(17), 9155–9206.
156 D. M. Lienhard *et al.*, 2012, submitted.
157 E. Andrews and S. M. Larson, *Environ. Sci. Technol.*, 1993, **27**(5), 857–865.
158 F. D. Pope, B. J. Dennis-Smither, P. T. Griffiths, S. L. Clegg and R. A. Cox, *J. Phys. Chem. A*, 2010, **114**(16), 5335–5341.
159 J. Wagner, E. Andrews and S. M. Larson, *J. Geophys. Res.*, 1996, **101**(D14), 19533–19540.
160 J. M. Lightstone, T. B. Onasch, D. Imre and S. Oatis, *J. Phys. Chem. A*, 2000, **104**(41), 9337–9346.
161 S. T. Martin, J. C. Schlenker, A. Malinowski, H. M. Hung and Y. Rudich, *Geophys. Res. Lett.*, 2003, **30**(21).
162 I. N. Tang, H. R. Munkelwitz and J. G. Davis, *J. Aerosol Sci.*, 1978, **9**, 505–511.
163 R. A. Robinson and R. H. Stokes, *Electrolyte solutions*, Dover Publications, Mineola, NY, 2002, 2nd rev. edn, p. 571p xv, .
164 C. Peng, M. N. Chan and C. K. Chan, *Environ. Sci. Technol.*, 2001, **35**(22), 4495–4501.
165 C. G. Peng and C. K. Chan, *Atmos. Environ.*, 2001, **35**(7), 1183–1192.
166 F. D. Pope, *et al.*, *J. Aerosol Sci.*, 2010, **41**(5), 457–467.
167 M. N. Chan, S. M. Kreidenweis and C. K. Chan, *Environ. Sci. Technol.*, 2008, **42**(10), 3602–3608.
168 C. G. Peng, A. H. L. Chow and C. K. Chan, *Aerosol Sci. Technol.*, 2001, **35**(3), 753–758.
169 A. K. Ray, R. D. Johnson and A. Souyri, *Langmuir*, 1989, **5**(1), 133–140.
170 M. Y. Choi and C. K. Chan, *J. Phys. Chem. A*, 2002, **106**(18), 4566–4572.
171 H. S. Na, S. Arnold and A. S. Myerson, *J. Cryst. Growth*, 1995, **149**(3–4), 229–235.
172 M. Kanakidou, *et al.*, *Atmos. Chem. Phys.*, 2005, **5**, 1053–1123.
173 A. M. Middlebrook, D. M. Murphy and D. S. Thomson, *J. Geophys. Res.*, 1998, **103**(D13), 16475–16483.
174 S. H. Lee, D. M. Murphy, D. S. Thomson and A. M. Middlebrook, *J. Geophys. Res.-Atmos.*, 2002, **107**(D1–D2), 4003.
175 M. N. Chan and C. K. Chan, *Atmos. Chem. Phys.*, 2005, **5**, 2703–2712.
176 A. S. Wexler and S. L. Clegg, *J. Geophy. Res.-Atmos.*, 2002, **107**(D14).
177 S. L. Clegg, M. J. Kleeman, R. J. Griffin and J. H. Seinfeld, *Atmos. Chem. Phys.*, 2008, **8**(4), 1057–1085.
178 A. Zuend, C. Marcolli, B. P. Luo and T. Peter, *Atmos. Chem. Phys.*, 2008, **8**(16), 4559–4593.
179 I. N. Tang, *J. Geophys. Res.*, 1997, **102**(D2), 1883–1893.
180 S. L. Clegg, S. S. Ho, C. K. Chan and P. Brimblecombe, *J. Chem. Eng. Data*, 1995, **40**(5), 1079–1090.
181 I. N. Tang and H. R. Munkelwitz, *J. Appl. Meteorol.*, 1994, **33**(7), 791–796.
182 A. B. Zdanovskii, *Z. Fiz. Khim.*, 1948, **22**(12), 1478–1485.
183 A. B. Zdanovskii, *Z. Fiz. Khim.*, 1948, **22**(12), 1486–1495.
184 R. H. Stokes and R. A. Robinson, *J. Phys. Chem.*, 1966, **70**(7), 2126.
185 G. Hargreaves, *et al.*, *J. Phys. Chem. A*, 2010, **114**(4), 1806–1815.
186 J. R. Butler, L. Mitchem, K. L. Hanford, L. Treuel and J. P. Reid, *Faraday Discuss.*, 2008, **137**, 351–366.

187 K. L. Hanford, *et al.*, *J. Phys. Chem. A*, 2008, **112**(39), 9413–9422.
188 D. O. Topping, G. B. McFiggans and H. Coe, *Atmos. Chem. Phys.*, 2005, **5**, 1205–1222.
189 J. S. Walker, *et al.*, *J. Phys. Chem. A*, 2010, **114**, 12682–12691.
190 G. B. Erdakos and J. F. Pankow, *Atmos. Environ.*, 2004, **38**(7), 1005–1013.
191 N. O. A. Kwamena, J. Buajarern and J. P. Reid, *J. Phys. Chem. A*, 2010, **114**(18), 5787–5795.
192 J. Buajarern, L. Mitchem and J. P. Reid, *J. Phys. Chem. A*, 2007, **111**(37), 9054–9061.
193 J. Buajarern, L. Mitchem and J. P. Reid, *J. Phys. Chem. A*, 2007, **111**(46), 11852–11859.
194 M. Guillon, R. E. H. Miles, J. P. Reid and D. McGloin, *New J. Phys.*, 2009, **11**, 103041.
195 L. Mitchem, J. Buajarern, A. D. Ward and J. P. Reid, *J. Phys. Chem. B*, 2006, **110**(28), 13700–13703.
196 V. Zelenay, *et al.*, *J. Aerosol Sci.*, 2011, **42**(1), 38–51.
197 T. L. Threlfall, *Analyst*, 1995, **120**(10), 2435–2460.
198 M. C. Yeung, T. Y. Ling and C. K. Chan, *J. Phys. Chem. A*, 2010, **114**(2), 898–903.
199 D. Ehre, *et al.*, *Cryst. Growth Des.*, 2011, **11**(10), 4572–4580.
200 H. B. Wu, M. N. Chan and C. K. Chan, *Aerosol Sci. Technol.*, 2007, **41**(6), 581–588.
201 H. B. Wu and C. K. Chan, *Atmos. Environ.*, 2008, **42**(2), 313–322.
202 T. Y. Ling and C. K. Chan, *Environ. Sci. Technol.*, 2007, **41**(23), 8077–8083.
203 I. N. Tang and K. H. Fung, *J. Chem. Phys.*, 1997, **106**(5), 1653–1660.
204 J. F. Pankow, *Atmos. Environ.*, 1994, **28**(2), 185–188.
205 S. L. Clegg and J. H. Seinfeld, *J. Phys. Chem. A*, 2006, **110**(17), 5692–5717.
206 Y. Nannoolal, J. Rarey and D. Ramjugernath, *Fluid Phase Equilib.*, 2008, **269**(1–2), 117–133.
207 S. Compernolle, K. Ceulemans and J. F. Muller, *Atmos. Chem. Phys.*, 2011, **11**(18), 9431–9450.
208 M. Bilde, I. Riipinen, C. Cappa and N. Donahue, *et al.*, *Atmos. Chem. Phys. Discuss.*, 2012, to be submitted.
209 A. J. Huisman, U. K. Krieger, A. Zuend, C. Marcolli and T. Peter, *Geophys. Res. Lett.*, 2012, in preparation.
210 L. Monchick and H. Reiss, *J. Chem. Phys.*, 1954, **22**(5), 831–836.
211 T. S. Baynes, *The Encyclopaedia Britannica, a dictionary of arts, sciences, and general literature*, C. Scribner's sons, New York, 9th edn, 1878, vol. 7.
212 N. A. Fuchs, *Evaporation and droplet growth in gaseous media*, Pergamon Press, London, 1959, p. 72.
213 E. J. Davis, P. Ravindran and A. K. Ray, *Chem. Eng. Commun.*, 1980, **5**(5–6), 251–268.
214 N. A. Fuchs and A. G. Sutugin, *Highly dispersed aerosols*, Ann Arbor Science Publishers, Ann Arbor, 1970, p. 105.
215 H. R. Pruppacher and J. D. Klett, *Microphysics of clouds and precipitation*, Kluwer Academic Publishers, Dordrecht, Boston, 2nd rev. and enl. edn, 1997, p. 506.
216 E. J. Davis and A. K. Ray, *J. Chem. Phys.*, 1977, **67**(2), 414–419.
217 H. W. Xue, A. M. Moyle, N. Magee, J. Y. Harrington and D. Lamb, *J. Atmos. Sci.*, 2005, **62**(12), 4310–4326.
218 A. K. Ray and S. Venkatraman, *AIChE J.*, 1995, **41**(4), 938–947.
219 T. M. Allen, D. C. Taflin and E. J. Davis, *Ind. Eng. Chem. Res.*, 1990, **29**(4), 682–690.
220 H. H. Tu and A. K. Ray, *Chem. Eng. Commun.*, 2005, **192**(4), 474–498.
221 M. Trunk, J. Popp and W. Kiefer, *Chem. Phys. Lett.*, 1998, **284**(5–6), 377–381.
222 F. D. Pope, *et al.*, *J. Phys. Chem. A*, 2010, **114**(37), 10156–10165.
223 S. Holler, *et al.*, *Opt. Lett.*, 1998, **23**(18), 1489–1491.
224 J. M. Prausnitz, R. N. Lichtenthaler and E. G. d. Azevedo, *Molecular thermodynamics of fluid-phase equilibria*, Prentice Hall PTR, Upper Saddle River, NJ, 3rd edn, 1999, p. 860, p xxiii.
225 M. Bilde, B. Svenningsson, J. Monster and T. Rosenorn, *Environ. Sci. Technol.*, 2003, **37**(7), 1371–1378.
226 C. D. Cappa, E. R. Lovejoy and A. R. Ravishankara, *J. Phys. Chem. A*, 2007, **111**(16), 3099–3109.
227 T. Koop, J. Bookhold, M. Shiraiwa and U. Poeschl, *Phys. Chem. Chem. Phys.*, 2011, **13**(43), 19238–19255.
228 B. J. Murray, *et al.*, *Nat. Geosci.*, 2010, **3**(4), 233–237.
229 C. D. Cappa, W. S. Drisdell, J. D. Smith, R. J. Saykally and R. C. Cohen, *J. Phys. Chem. B*, 2005, **109**(51), 24391–24400.
230 S. M. Kreidenweis, *et al.*, *J. Geophys. Res.*, 2003, **108**(D7), 4213.
231 M. Shiraiwa, M. Ammann, T. Koop and U. Poeschl, *Proc. Natl. Acad. Sci. U. S. A.*, 2011, **108**(27), 11003–11008.
232 M. Zientara, D. Jakubezyk, K. Kolwas and M. Kolwas, *J. Phys. Chem. A*, 2008, **112**(23), 5152–5158.
233 M. Gershenzon, *et al.*, *J. Phys. Chem. A*, 2004, **108**(9), 1567–1573.
234 Y. Q. Li, *et al.*, *J. Phys. Chem. A*, 2001, **105**(47), 10627–10634.
235 W. S. Drisdell, C. D. Cappa, J. D. Smith, R. J. Saykally and R. C. Cohen, *Atmos. Chem. Phys.*, 2008, **8**(22), 6699–6706.
236 W. S. Drisdell, R. J. Saykally and R. C. Cohen, *Proc. Natl. Acad. Sci. U. S. A.*, 2009, **106**(45), 18897–18901.
237 W. S. Drisdell, R. J. Saykally and R. C. Cohen, *J. Phys. Chem. C*, 2010, **114**(27), 11880–11885.
238 P. M. Winkler, *et al.*, *J. Geophys. Res.*, 2006, **111**(D19), D19202.
239 P. M. Winkler, *et al.*, *Phys. Rev. Lett.*, 2004, **93**(7), 075701.
240 R. E. H. Miles, K. J. Knox, J. P. Reid, A. M. C. Laurain and L. Mitchem, *Phys. Rev. Lett.*, 2010, **105**, 116101.
241 D. L. Bones, J. P. Reid, D. M. Lienhard and U. K. Krieger, *Proc. Natl. Acad. Sci. U. S. A.*, 2012, in press.
242 J. F. Hamilton, *et al.*, *Atmos. Chem. Phys.*, 2011, **11**(12), 5917–5929.
243 B. J. Turpin, P. Saxena and E. Andrews, *Atmos. Environ.*, 2000, **34**(18), 2983–3013.
244 J. J. Najera, C. J. Percival and A. B. Horn, *Phys. Chem. Chem. Phys.*, 2009, **11**(40), 9093–9103.
245 J. J. Najera, C. J. Percival and A. B. Horn, *Phys. Chem. Chem. Phys.*, 2010, **12**(37), 11417–11427.
246 H. M. Hung, Y. Katrib and S. T. Martin, *J. Phys. Chem. A*, 2005, **109**(20), 4517–4530.
247 P. J. Ziemann, *Faraday Discuss.*, 2005, **130**, 469–490.
248 M. D. King, K. C. Thompson and A. D. Ward, *J. Am. Chem. Soc.*, 2004, **126**(51), 16710–16711.
249 O. Vesna, M. Sax, M. Kalberer, A. Gaschen and M. Ammann, *Atmos. Environ.*, 2009, **43**(24), 3662–3669.
250 O. Vesna, *et al.*, *Atmos. Chem. Phys.*, 2008, **8**(16), 4683–4690.
251 M. D. King, K. C. Thompson, A. D. Ward, C. Pfrang and B. R. Hughes, *Faraday Discuss.*, 2008, **137**, 173–192.
252 F. D. Pope, P. J. Gallimore, S. J. Fuller, R. A. Cox and M. Kalberer, *Environ. Sci. Technol.*, 2010, **44**(17), 6656–6660.
253 L. P. Chan and C. K. Chan, *Aerosol Sci. Technol.*, 2012, **46**(7), 781–793.
254 C. Baduel, *et al.*, *Environ. Sci. Technol.*, 2011, **45**(12), 5238–5244.
255 B. D'Anna, *et al.*, *J. Geophys. Res.-Atmos.*, 2009, 114.
256 L. P. Chan and C. K. Chan, *Aerosol Sci. Technol.*, 2012, **46**(2), 236–247.
257 L. P. Chan and C. K. Chan, *Aerosol Sci. Technol.*, 2011, **45**(7), 872–883.
258 J. V. Sinfield, O. Colic, D. Fagerman and C. Monwuba, *Appl. Spectrosc.*, 2010, **64**(2), 201–210.
259 A. E. Carruthers, J. S. Walker, A. Casey, A. J. Orr-Ewing and J. P. Reid, *Phys. Chem. Chem. Phys.*, 2012, **14**, 6741–6748.

